Title

Hyporheic exchanges due to channel bed and width undulations

Authors

Movahedi, Neshat
Dehghani, Amir Ahmad
Schmidt, Christian
et al.

Publication Date

2021-03-01

DOI

10.1016/j.advwatres.2021.103857

Data Availability

The data associated with this publication are available upon request.

Peer reviewed

Hyporheic exchanges due to channel bed and width undulations

Neshat Movahedi[a], Amir Ahmad Dehghani[b,*], Christian Schmidt[c], Nico Trauth[d], Gregory Brian Pasternack[e], Michael J. Stewardson[f], Mehdi Meftah Halghi[g]

[a] PhD Candidate, Department of Water and Soil Engineering, Gorgan University of Agricultural Sciences and Natural Resources, Gorgan, Iran, neshat.movahedi@gau.ac.ir

[b] Associate Professor, Department of Water and Soil Engineering, Gorgan University of Agricultural Sciences and Natural Resources, Gorgan, Iran, *Corresponding author email: a.dehghani@gau.ac.ir

[c] Researcher, Department of Hydrogeology, Helmholtz Center for Environmental Research (UFZ), Leipzig, Germany, christian.schmidt@ufz.de

[d] Hydraulic Engineer, Bjoernsen Consulting Engineers (BCE), Leipzig, Germany, ntrauth@posteo.de

[e] Professor, Department of Land, Air and Water Resources, University of California, Davis, CA, USA, gpast@ucdavis.edu

[f] Professor, Department of Infrastructure Engineering, The University of Melbourne, Parkville VIC 3010, Australia, mjstew@unimelb.edu.au

[g] Associate Professor, Department of Water and Soil Engineering, Gorgan University of Agricultural Sciences and Natural Resources, Gorgan, Iran, meftah@gau.ac.ir

How to cite: Movahedi, N., Dehghani, A.A., Schmidt, C., Trauth, N., Gregory Brian Pasternack, G.B., Stewardson, M.J., Meftah Halghi, M. 2021. Advances in Water Resources. https://doi.org/10.1016/j.advwatres.2021.103857

Abstract

Riffle-pool sequences are fundamental, ubiquitous morphological features of alluvial rivers that are thoroughly studied in general and commonly incorporated into river restoration projects. Most previous investigations on the effect of riffle-pool sequences on hyporheic exchanges focused on solely bed undulation, because that is widely thought to be the defining feature of riffle-pool sequences. However, riffle- pool sequences also have significant width undulations that are vital to riffle-pool sequences morphodynamics, yet relatively few studies exist on the effect of such undulations on hyporheic exchanges. Thus, in this study based on laboratory experiments and numerical simulations, we investigate the effect of bed and width undulations on hyporheic zone characteristics for various ratio of width amplitude to bed amplitude. The variation of hyporheic exchange characteristics (i.e. hyporheic exchange flux and residence time) for different riffle-pool designs were also assessed by creating prescribed topography of synthetic river valleys. The results showed that due to pressure variation along width undulations, the upwelling and downwelling patterns can also be observed for only width undulations in rivers, in the absence of bed undulations, and as width undulation amplitude decreases, the normalized hyporheic exchanges (Q^*_{HZ}) increase and normalized median residence time (RT*) decreases. Also, simultaneous channel bed and width undulations result in higher Q^*_{HZ} especially when a pool is located in an expansion (aka "oversized" cross-section) and a riffle in a constriction ("nozzle"). Our results suggest that river restoration project that artificially construct wide pools and constricted riffles will achieve maximum Q^*_{HZ} and RT*, though they will not be geomorphically self-sustainable.

Keywords: bed undulation, width undulation, hyporheic exchanges, residence time

1. Introduction

Multiple definitions for hyporheic zone (HZ) have been proposed reflecting different purposes of previous studies (Ward 2016). In this study, HZ is defined as a saturated area beneath and adjacent to a river in which water can transfer into the riverbed to become subsurface flow and then return above the riverbed to be surface flow. This process of movement in and out of the bed is named hyporheic exchange (HE) (Tonina and Buffington 2011). When stream water flows into the subsurface, oxygen and nutrients transfer, benefiting many biogeochemical, ecological and biological processes (Battin et al. 2008, Bencala 2000, Boulton et al. 1998, Zheng et al. 2019).

Tonina and Buffington (2009) expressed a mechanism for HE based on three dominating drivers: spatial changes of energy head gradient, cross-sectional area of alluvium, and hydraulic conductivity. There is a clear mechanistic chain of cause and effect between local fluvial topography, HE, and ecological

functionality. In this study, we focused on the effect of spatial changes in the energy head gradient due to coherently varying river topography. River morphology, commonly quantified with planform, cross-section, and longitudinal profile metrics, represents a primary control on HE by affecting pressure amplitude variation. The following sections present a literature for the impact of river morphology on HE, and the objectives of this study.

1.1 Effects of Bed Undulations

Previous studies show that the main driver of HE is the pressure gradient along geomorphic features like bars, dunes and riffle-pool (RP) sequence (Buffington and Tonina 2009, Fehlman 1985, Thibodeaux and Boyle 1987, Tonina and Buffington 2009, Trauth et al. 2015). The upwelling and downwelling fluxes in HZ, induced by pressure gradients along RP sequences, will improve river habitat (Gariglio et al. 2013) and stimulate the denitrification process (Trauth et al. 2014). They are also common features of river restoration projects (Emery et al. 2003, Schwartz and Herricks 2007, Schwartz et al. 2015, Sear and Newson 2004, Whiteway et al. 2010), and therefore considered as the main focus of this study.

Few laboratory experiments and numerical simulations have investigated HE in RP morphologies. Tonina and Buffington (2007) studied HE in RP channels with alternate bars, through laboratory experiments and numerical simulations. The effects of flow discharge and bed form amplitude on HZ characteristics were investigated by injection of Fluorescein as a tracer to determine solute exchange between surface and subsurface flow. Their results showed that not only the bed form amplitude but also the interaction between bed form and discharge can drive HE. Trauth et al. (2013) investigated the effect of stream discharge and ambient groundwater on HZ characteristics for RP sequences with various amplitudes. Their numerical simulation results showed that HE increased with stream discharge and mean residence time decreased. Also, by increasing the RP amplitude, the HE increased and residence time decreased. Also, Zhou and Endreny (2013) investigated the effect of restoration structures on hyporheic exchanges rate and hyporheic penetration depth along sequences of RP. The results of flume experiments and numerical simulations in their study showed that restoration structures increased the hyporheic exchanges and decreased the penetration depth.

1.2 Effects of Width Undulations

Similar to bedforms, river irregular planform geometry also leads to formation of hyporheic zones along river banks (Cardenas 2009b). Flow convergence and divergence along channel width undulations affect pressure gradients and as a result drive HE. Cardenas (2009a) through 2D numerical simulations investigated the hyporheic fluxes along sinusoidal channel banks. His results showed that lateral hyporheic

fluxes increased by sinuosity where the stream has no net flux of water (neutral conditions). However, the impact of both channel flow and sinusoidal banks on HEs which lead to the formation of both horizontal and vertical fluxes was not considered in his study.

The effect of meander planform on HEs has been studied by many (Balbarini et al. 2017, Boano et al. 2006, Gomez-Velez et al. 2017, Han and Endreny 2014, Pescimoro et al. 2019, Peterson and Sickbert 2006, Revelli et al. 2008, Stonedahl 2011), but these studies all assume a constant channel width.

1.3 Coherent Bed and Width Undulations

Channel width undulations affect bed topography of many gravel bed rivers (Jacobson and Gran 1999). Literature shows that width undulations can create pools in width constrictions and riffles in width expansions (Bittner 1994, Buckrell 2017, De Almeida and Rodríguez 2012, Nelson et al. 2015, Repetto et al. 2002, Richards 1976a, White et al. 2010, Wu and Yeh 2005).

In natural systems, the locations of riffles and pools are frequently linked to planform geometry or the spatial pattern of river-corridor morphology. Many river rehabilitation projects aim to re-establish natural pool-riffle sequences (Brown et al. 2016, Lane et al. 2018); however, there are disagreements in the literature on the morphodynamic processes that shape them, and resultantly, there is no widely adapted, standardized, systems approach for their design (Brown and Pasternack 2019, Wade et al. 2002). To increase river channel stability and quality of aquatic habitat, pool-riffle sequences are being artificially constructed, so considering form-process interactions during restoration projects is vital (Schwindt et al. 2020).

During in-channel discharges, near-bed velocity and shear stress are lower in pools than riffles, but during floods (usually 1-2 times bankfull discharge) the location of peak velocity “reverses” such that near-bed velocity and shear stresses are higher in the pool than over riffle (De Almeida and Rodríguez 2011, Pasternack et al. 2008). Pool aggradation and riffle erosion (or just riffle armoring) during low discharge and pool scour and riffle aggradation at high discharge in gravel-bed systems yields a morphodynamic mechanisms responsible for the self-maintenance of pools and riffles (De Almeida and Rodríguez 2011, Pasternack et al. 2018b, Strom et al. 2016).

Considering that riffles generally are shallower and pools deeper, higher mean velocities in a pool are only possible in situations where the shape of the pool’s cross section is more constricted than that of the riffle (Pasternack et al. 2018a). However, this is often not minded in actual engineering construction practice. During engineered channelization, pool-riffle structure is often modified with excavators. These machines usually site on the bank adjacent to the pool and need to pull the bucket perpendicular to the channel to dig

the pool. This strategy often yields a wider, deeper pool than suitable to have a velocity reversal. The problem could be resolved if project designers and construction crews were mindful of the simple Caamaño criterion. Caamaño et al. (2009) provided a simplified one-dimensional criterion in which velocity reversal occurrence is a function of residual pool depth, the ratio of riffle to pool depth, and the flow depth over a riffle. So, the question is that how the location of RP against channel width undulations can affect HE?

1.4 Study Objectives

As mentioned, many studies only characterized HE processes at RP sequences due to bed undulations and little is known about effect of width undulation on HZ characteristics. Also, to our knowledge, no study has yet considered the effect of relative width of pools and riffles. Some rivers meander over long distances with a constant width, but many rivers do have regular width undulations, and they are phased coherently with bed undulations. So, building on the first goal of the study to assess width undulations in isolation, the second goal of our study was to investigate the simultaneous effect of channel bed and width undulations on HZ characteristics. For the second goal, two scenarios were studied, in order to investigate the interaction of RP location and width undulations. In the first scenario, the pool was deep but constricted and then riffle was shallow but wide, and in the second scenario, the pool was both deep and wide (i.e. "oversized"), while the riffle was narrow and shallow (i.e. "nozzle"). These alternatives have been thoroughly studied for their geomorphic effects (Brown et al. 2016, Jackson et al. 2015, Pasternack et al. 2018a, b), but not for their HZ characteristics. So, in order to generalize results for large scale cases, the configurations studied by Brown et al. (2016) for investigating bed shear stress along the sequences of expansion-constriction widths, with riffle-pool sequences and also with flat bed, were examined numerically. In general, the following questions are addressed in this study:

- How HZ characteristics will be affected by only width undulations amplitude (Δ_{wu})?

- How HZ characteristics will be affected by width undulations amplitude (Δ_{wu}) for a given bed undulations amplitude (Δ_{bu})?

- How HZ characteristics will be affected by relative location of RP over width undulations?

- Does the above results can also be found in large scale case?

For the above goals, a series of laboratory experiments and numerical simulations were performed to characterize HE processes due to width undulations and also bed undulations with considering synchronous width undulations. For each case, the hydraulic heads along sediment water interface (SWI) were coupled with a groundwater model, and then a particle tracking method was used to derive HZ characteristics, i.e. hyporheic exchanges flow (Q_{HZ}), residence time (RT) and hyporheic depth (d_{HZ}). The novelty of this study

is that it provides the first assessment of investigating synchronous bed and width undulations in gravel bed rivers with RP morphology which is a hotspot for microorganism living in HZ and widely constructed in river restoration projects.

2. Experimental Design

In order to meet study goals, a combination of laboratory experiments and numerical simulations were performed with various ratios for amplitude of channel width and bed undulations. In the following sections, after introducing the effective parameters within dimensional analysis, the laboratory experiments and numerical simulations will be explained in detail.

2.1 Dimensional Analysis

Generally, hyporheic zone characteristics including hyporheic exchanges flow (Q_{HZ}), residence time (RT) and hyporheic exchange depth (d_{HZ}) can be express as a function of the following parameters:

$$(Q_{HZ}, RT, d_{HZ}) = f(V, h, K, d_{50}, n, \rho, \mu, \lambda, \Delta_{bu}, \Delta_{wu}, A_S) \quad (1)$$

where f = the unknown function, V = mean flow velocity (m/s), h = mean flow depth (m), K = hydraulic conductivity (m/s), d_{50} = the median sediment size (m), n = porosity, ρ = the water density (kg/m^3), μ = dynamic viscosity, λ = wavelength of bed or width undulations (m), Δ_{bu} = amplitude of bed undulations (m) (riffle crest to pool trough), Δ_{wu} = amplitude of width undulations (m), A_S = surface and subsurface interface area (m^2). By applying the Buckingham π theorem to eq. (1), the dimensionless relationship becomes:

$$f\left(\frac{Q_{HZ}}{K\times\lambda^2}, \frac{RT\times K}{\lambda}, \frac{d_{HZ}}{\lambda}, , \frac{V}{K}, \frac{h}{\lambda}, \frac{\mu}{\rho K\lambda}, \frac{\Delta_{bu}}{\lambda}, \frac{\Delta_{wu}}{\lambda}, \frac{\lambda^2}{A_s}, \frac{d_{50}}{\lambda}, n\right) = 0 \quad (2)$$

Due to the use of one sediment size, and a constant porosity and wavelength, the last two terms of above equation can be omitted. Combining the rest of dimensionless parameters, the following equation is obtained:

$$f\left(\frac{Q_{HZ}}{K\times A_s}, \frac{RT\times K}{\lambda}, \frac{d_{HZ}}{\lambda}, \frac{\rho V h}{\mu}, \frac{\Delta_{wu}}{\Delta_{bu}}\right) = 0 \quad (3)$$

2.2 Laboratory Experiments

Experiments were conducted in a straight recirculating flume, 12 m long, 1 m wide and 1 m deep. The flow was supplied in the flume by a centrifugal pump and the discharge was measured with an ultrasonic flow-meter. The sediment bed was a mixture of gravels and sands with a median diameter of 6.8 mm, a geometric

standard deviation of $\sigma_g = \sqrt{d_{84}/d_{16}} = 1.5$, a porosity of 0.34. The water and sediment elevations were measured by a digital point gage (resolution ± 0.1 mm). The velocity measurement was done by micro-propeller. The following sections introduce the geometry of laboratory models.

2.2.1 Width Undulations

The first part of laboratory experiments was conducted to investigate the effect of width undulations on HZ characteristics. Hereinafter the expansion-constriction scenarios without bed forms are named "EC scenarios". Five sequences of sinusoidal width undulations were created by Polystyrene sheets (Figure 1a) cut with a hotwire system based on the following equation:

$$y(x) = \frac{\Delta_{wu}}{2} \sin(\lambda x) \quad (4)$$

where x and y are distance along flume length and width, respectively. The wavelength and amplitude were one meter and 0.125 m respectively for these laboratory experiments which lead to the ratio of constriction width to expansion width equal to the 0.7. This ratio is consistent with the natural conditions of rivers with a riffle-pool morphology (Bayat et al. 2017, Nelson et al. 2015, Wu and Yeh 2005).

2.2.2 Bed and Width Undulations

To assess the simultaneous effect of channel bed and width undulations on HZ characteristics, RP sequences were constructed in two scenarios. For one scenario, pools were located in narrower (constricted) areas and riffle in wider (expansion) areas, which hereafter named as "pool constriction riffle expansion" (PCRE) scenarios. For the vice versa phasing of width and bed undulations the name used was "pool expansion riffle constriction" (PERC). RPs were shaped by means of wooden rib in the expansion-constriction channel according to the following equation:

$$z(x) = \frac{\Delta_{bu}}{2} \sin(\lambda x) \quad (5)$$

where x and z are distance along flume width and depth, respectively. The wavelength of RP sequences was equal to 1 m and the bed amplitude was 0.068 m. Selection of wavelength value was based on the Montgomery et al. (1995) results for channel width formed in rivers with large wood. Also, bed form amplitude was chosen to yield a ratio of bed form amplitude to wavelength set within the range of values observed for natural RP systems (Buffington and Montgomery 1999).

The wavelength of both bed and width undulations was 1 m. The bed and width amplitudes were 0.068 m and 0.125 m, respectively which led to the Δ_{wu}/Δ_{bu}=1.84 (Table 1). Figure 1b shows the bed and width undulations formed in the channel for PCRE scenario.

2.2.3 Experimental Procedure

After construction of each model, the water was supplied through the flume by a centrifugal pump. The downstream gate was held up, in order to completely saturate the sediments. Then, the discharge was increased to the desired value and the downstream gate completely lowered to create the underflow conditions.

As this study aims to quantify how the expansion and contraction of width in a riffle-pool river affects the hyporheic exchanges characteristics, the following assumptions and limitations are used in this study:

1- The flow is non-uniform since we have bed or width undulation.

2- The flow is steady state and the approach flow is clear and does not contain sediment.

3- The channel banks are assumed to be non-erodible to avoid the effect of inter-meander HE on the results.

The flow depths and velocities were measured for all scenarios. The reference level for measuring flow depth and flow velocity was the mean bed amplitude. The monitoring section was located at the middle bed or width undulations which water surface elevations were measured every 5 cm along flume length, and every 10 cm along flume width. Also, the streamwise velocities (U) were measured at five cross sections.

It should be noted, in order to observe hyporheic paths against the flume glass wall, through the width undulation scenarios, only half of the width undulations were constructed in the laboratory (Figure 1). Surface-subsurface exchange was visualized by injecting dye in different positions into the sediments and drawing the penetration paths on the flume glass wall through the time.

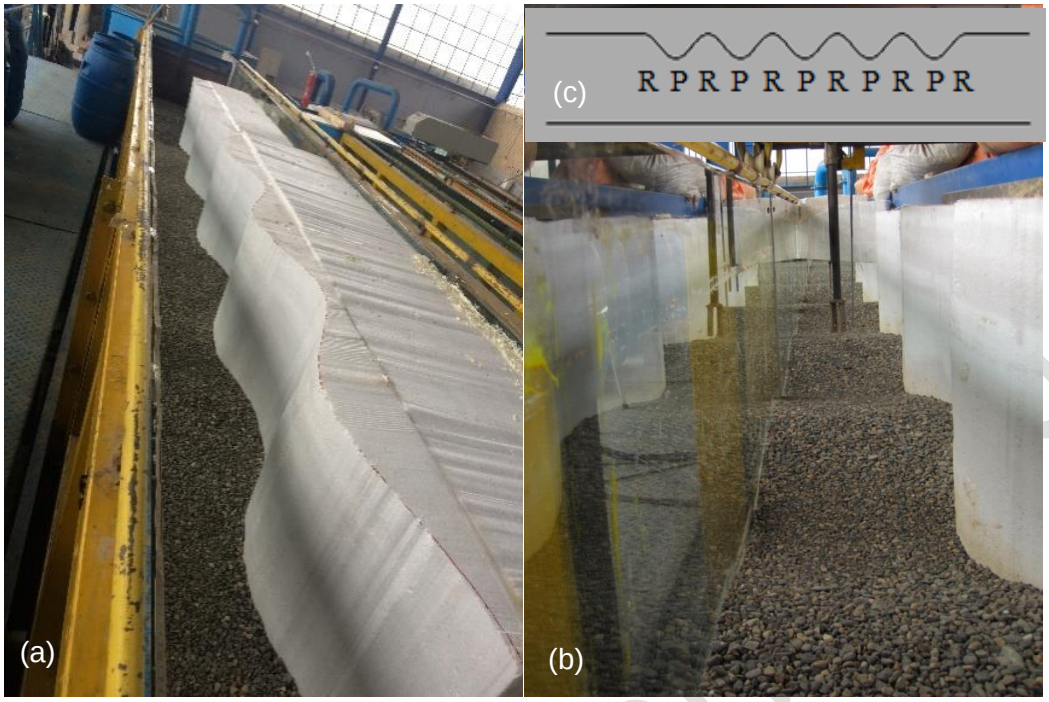

Figure 1. Channel bank undulations with (a) only width undulations with (EC scenario); (b) bed and width undulations: Pool in Constriction and Riffle in Expansion (PCRE scenario); and (c) plan view of PCRE.

Table 1. The geometry of models in laboratory experiments and numerical simulation scenarios

Study frameworks	Scenarios	Δ_{wu} (m)	Δ_{bu} (m)	Δ_{wu}/Δ_{bu}
Laboratory and numerical simulation validation	EC	0.125	-	-
	PCRE PERC	0.125	0.068	1.84
Numerical simulation prediction	EC	0.06, 0.09, 0.17	-	-
	RP	-	0.068	-
	PCRE PERC	0.06, 0.09, 0.17	0.068	0.88, 1.32, 2.5
Numerical simulation (prescribed bed topography of Brown et al. (2016))	S2	7	-	-
	S3	-	1	-
	S4	7	1	7
	S5			

2.3 Numerical Models

Two sets of numerical simulations were performed. First, numerical simulations were done for laboratory experiments with careful measurements enabling model validation for free surface and subsurface flow (Table 1). Then, after assessing the accuracy of the simulation model, additional numerical models were performed with different ratios of width amplitude to bed amplitude (i.e. Δ_{wu}/Δ_{bu} =0.88, 1.32 and 2.5) for all EC, PCRE and PERC scenarios, as well as the RP case with only bed undulation. The combination of experimental results and numerical simulations provides valuable insight into hyporheic phenomena.

Second, numerical simulations were done to compare results to field scale cases. For this purpose, the study used the systematically varied configurations developed by Brown et al. (2016) for studying the effects of bed and width undulations on bed shear stress along RP sequences (i.e. S2, S3, S4 and S5 in Table 1 and Figure 2). These were built using the synthetic river valley (SRV) concept and software of Brown et al. (2014) based on hydraulic, sedimentary and geometry data. The river length and width were 2358 and 70 m, respectively. Bank and bed wavelengths were 196 m and the discharge was 125 m^3/s.

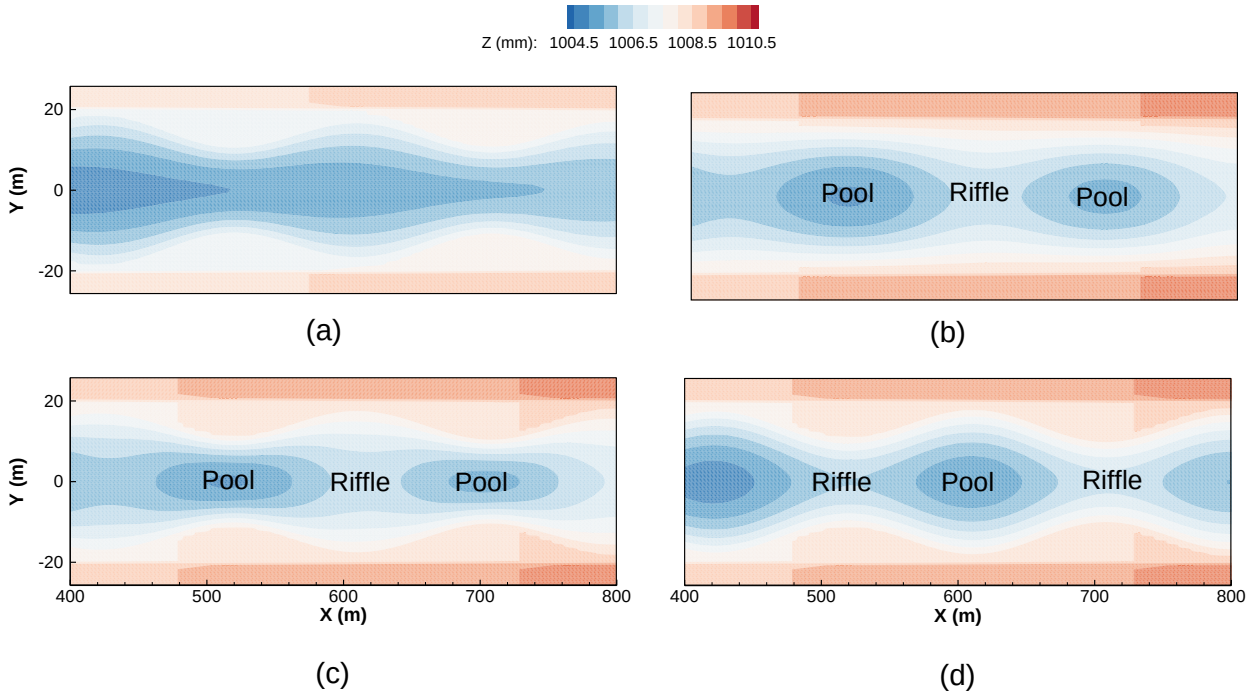

Figure 2. Plan view of bed topographies created by synthetic river valley method (Brown et al., 2014), (a) S2 (Expansion constriction sequence, EC scenario); (b) S3 (Riffle pool sequence, RP scenario); (c): S4 (Pool in Constriction and Riffle in Expansion, PCRE scenario); and (d) S5 (Pool in Expansion and Riffle in Constriction, PERC scenario).

2.3.1 Surface Flow Model

The surface flow simulations for all scenarios, were performed with Open Source Field Operation and Manipulation (OpenFOAM) version 2.3.0, which employs the finite volume method (Greenshields 2015). The two-phase solver named interFOAM, with the Large Eddy Simulation (LES) method for turbulence closure was used. The interFoam solver is a transient solver for incompressible flow that was used with open channel flow and Free Surface Model (Farshi et al. 2018, Jellesma 2013, Shaheed 2016). For two-phase flow simulation in this solver, one fluid model was used, which only needs one series of equations for both phases. This solver uses the Volume of Fluid method for determining free water surface (the boundary between the water and air) which depends on determining the fraction of each fluid in every cell of the computational mesh (Shaheed 2016). The equation of volume fraction is:

$$\partial\alpha/\partial t+\nabla.(\alpha\, U)=0 \tag{6}$$

Where U is velocity field and α is volume fraction of water and air. The value of α is one for liquid phase, zero for air phase and between zero to one for the interphase. Equation (6) is also named as the interphase transport equation.

The density of the fluid inside each cell could be determined by volume fraction, which is also known as the phase fraction α (Shaheed 2016):

$$\rho = \alpha\rho_w + (1+\alpha)\rho_a \tag{7}$$

where ρ_a and ρ_w are density of air and water, respectively.

The constant-density continuity equation and the momentum equation can be expressed as Eq.(8) and Eq.(9), respectively :

$$\frac{\partial}{\partial t}(\rho) + \nabla(\rho\bar{U}) = 0 \Rightarrow \nabla(\bar{U}) = 0 \tag{8}$$

$$\frac{\partial(\rho\overline{U})}{\partial t} + \nabla.(\rho\bar{U}\bar{U}) = -\nabla p + \nabla.\left(\mu((\nabla\bar{U})^T + \nabla\bar{U})\right) + F_\sigma \tag{9}$$

The expression $\overline{UU}$ is Reynolds stress tensor. In the right hand of the above equation p is pressure, the second terms are turbulent and viscose stresses, and the last term is the surface tension force. The surface tension is modelled as continuum surface force ($F_\sigma = \sigma\kappa\nabla\sigma$), which σ is the surface tension constant and κ the curvature and can be approximated as:

$$\kappa = -\nabla.\left(\frac{\nabla\alpha}{|\nabla\alpha|}\right) \tag{10}$$

Due to this fact that the application of 3D models for field-scale simulations is computationally expensive, SRH-2D model, which solved the depth-averaged St. Venant equations was used to simulate free surface flow characteristics for scenarios S2, S3, S4 and S5.

2.3.2 Subsurface Flow Model

Subsurface flow was simulated using MODFLOW which solves the governing equations based on finite difference method (McDonald and Harbaugh 1988):

$$\frac{\partial}{\partial x}\left[K_{xx}\frac{\partial H}{\partial x}\right]+\frac{\partial}{\partial y}\left[K_{yy}\frac{\partial H}{\partial y}\right]+\frac{\partial}{\partial z}\left[K_{zz}\frac{\partial H}{\partial z}\right]+W=S_s\frac{\partial H}{\partial t} \quad (11)$$

where K_{xx}, K_{yy} and K_{zz} are hydraulic conductivity in x, y and z direction, respectively. H represents the hydraulic head, W the volumetric flux, S_s the specific storage of the porous media and t the time. The calculations were performed in hexahedral cells and the flow into and out of each cell was calculated using Darcy's equation:

$$Q=KA_l\frac{H_l-H_0}{r} \quad (12)$$

where Q is the volumetric fluid discharge from the neighbor into the cell, K is the hydraulic conductivity in the direction of flow, A_1 is the area of the shared side of the cell, r is the distance between the centers of the cells, H_1 is the hydraulic head associated with the neighboring cell, and H_0 is the cell in unknown head.

2.3.3 Boundary Conditions and Mesh Design

The upstream and downstream sides of the free surface domain boundary conditions used a spatially periodic pressure condition, so that our domain approximates a repeating domain in the flow direction (from upstream to downstream). The right and left faces (relative to the flow direction) are considered symmetry boundaries. A symmetry boundary (i.e., no flux) is applied at the top face of the water column. A no-slip wall boundary is set at the bottom face of free surface interface.

For surface simulations, the mesh was constructed within the blockMesh dictionary in OpenFOAM, such that the hexahedral horizontal cell size was 0.02×0.02 m^2 square. In the vertical direction, a higher density of grid nodes was applied for cells close to the SWI. The number of structured grid nodes of the whole domain varied from about 330,000 to near 460,000 depending on the geometric conditions.

For subsurface simulations in MODFLOW, calculations were performed in hexahedral cells using more than 180,840 and 378,777 elements for laboratory experiments scenarios and S series scenarios, respectively. Porous-domain boundary conditions are represented in Figure 3. The thickness of porous domain for experimental and for S scenarios was 0.34 m and 126 m, respectively. The sediment thickness

is adequately large that it no longer has an effect on the flow field near the SWI. We used Tonina & Buffington's suggestion as a first assumption, and then we examined this assumption by checking the pathlines whether they reached to the bottom of the domain or not. Tonina and Buffington (2011) suggested that depth of alluvium has a substantial effect on hyporheic flow when alluvial depth is less than a third of the bed form wavelength. So, this criterion was considered in selecting the thickness of the porous domain. Also, the porosity and hydraulic conductivity were considered as 0.3 and 5.6E-4 m/s, respectively, based on 119 reach measurements in French rivers by (Stewardson et al. 2016).

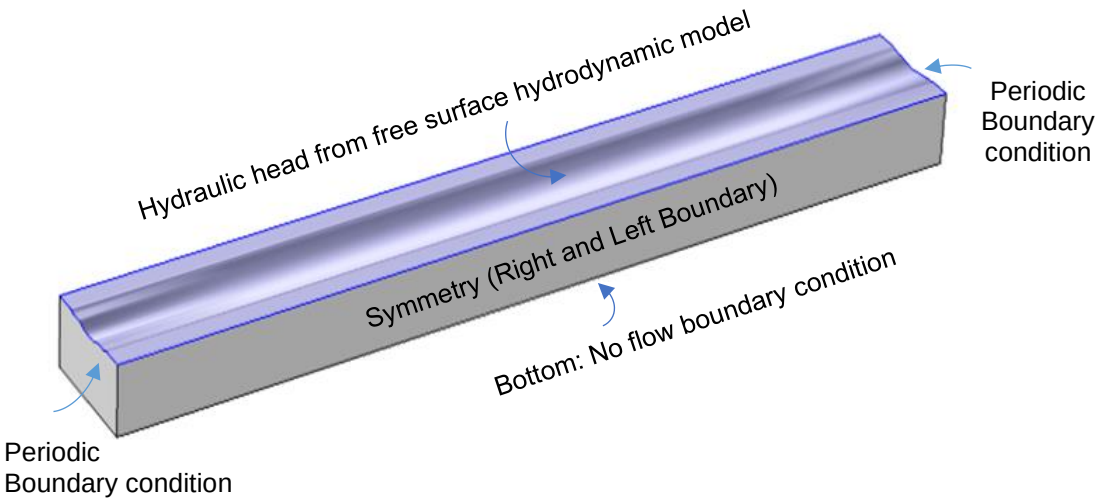

Figure 3. Boundary conditions of porous domain for subsurface flow simulation.

2.4 Data Analysis

In all numerical scenarios, turbulent flow characteristics in the water column were simulated by solving Reynolds-Averaged Navier-Stokes equations and a steady state groundwater flow model was applied for the underlying permeable sediment. These two sets of equations were coupled through the hydraulic head distribution along the SWI which was obtained from simulating of free surface flow. This one-way sequential coupling approach captures only flow from the surface water domain into the porous domain and does not account for feedbacks from subsurface flow into the surface water domain. However, hyporheic water that enters the stream channel is only a small volume fraction of the total stream discharge and hence has negligible impacts on hydrodynamic flow in the channel (Cheng and Chiew 1998, Prinos 1995). The literature review in the field of HE modeling have focused on surface-subsurface coupled models. The main reason that relatively high velocities in the free surface flow, whereas the velocities in the groundwater are

usually several orders of magnitude smaller, leading to different applied equations for the stream and the subsurface. Then, the MODPATH particle tracking method in MODFLOW was used to extract path lines and residence times of fluid particles in the middle topographic cycle, which was far enough from the inlet and outlet, so that boundary conditions could not affect results. In the particle tracking results analysis, only particles that entered the streambed from surface flow, remained in the streambed for a while, and then returned to surface flow from the streambed were considered in calculations. Hyporheic exchanges flow (Q_{HZ}) and median residence time (MRT) are normalized by the following equations:

$$Q^*_{HZ} = \frac{Q_{HZ}}{K \times A_s} \quad (15)$$

$$RT^* = \frac{MRT \times K}{\sigma_\lambda} \quad (16)$$

where σ_λ is the arc length along the sinusoidal width (Cardenas 2009a) which is different for each ratio of Δ_{wu}/Δ_{bu}. Since the particles travel in a three-dimensional space, the longitudinal and lateral travel distance were calculated based on initial and final coordinate of particles. In the following, we first report results of numerical model validation using laboratory data. For surface flow model validation, the observed and simulated water surface elevations and velocity distributions were compared. To quantitatively evaluate the accuracy of the numerical models, the efficiency of model validation, the root mean square error (RMSE) and mean percentage error (MPE) indexes were used:

$$RMSE = \sqrt{\sum_{i=1}^{n} \frac{(O_i - S_i)^2}{n}} \quad (13)$$

$$MPE = \frac{\sum_{i=1}^{n} \frac{O_i - S_i}{O_i}}{n} \times 100 \quad (14)$$

where O_i, S_i and n refer to the observed value, simulated value and number of samples, respectively.

Also, for validation of subsurface model, the emergence locations of injected dye for laboratory and field numerical simulations were compared.

Results are presented and discussed for four scenarios named as RP, EC, PCRE and PERC. For the last three scenarios, four ratios of Δ_{wu}/Δ_{bu} were compared for HZ characteristics (one ratio in both laboratory and numerical experiments, and three more ratios with only numerical simulations).

3. Results

3.1 Model Validation Results

3.1.1 Surface Flow

The OpenFOAM results were verified for surface flow using the laboratory observations. Comparison of observed versus simulated water surface elevations and streamwise velocities showed a good agreement (Figure 4). The observed water surface elevations and velocities agreed well with the simulated one with the overall RMSE of 0.0034 m and 0.07 m/s, and also MPE of 3.55% and 15.31%, respectively (Table 2).

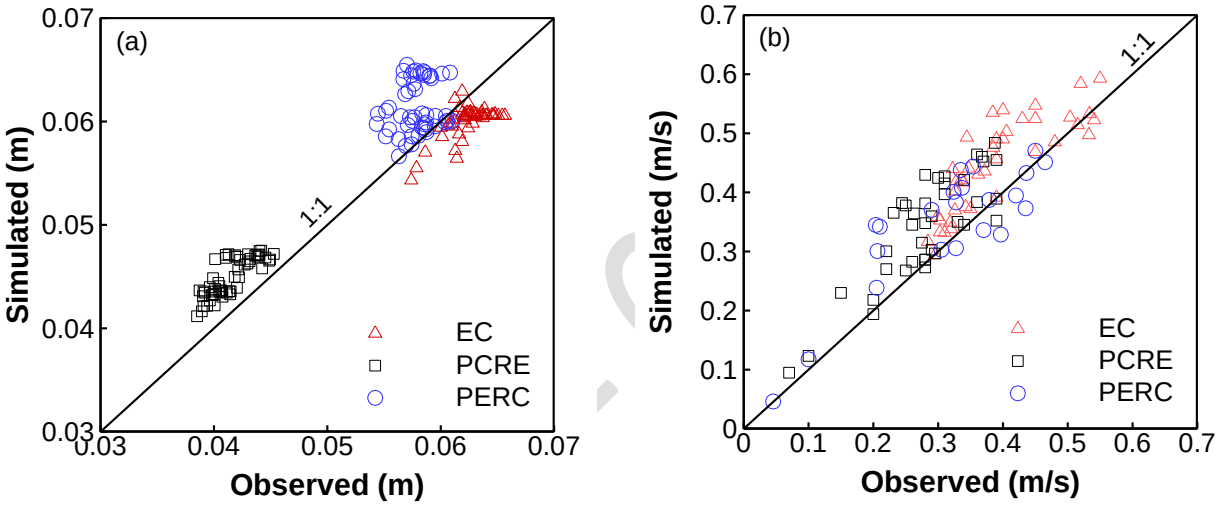

Figure 4. Comparison of observed versus simulated (a) water surface elevations; and (b) streamwise velocities.

Table 2. Model performance metrics for water surface elevation and velocity

	Water Surface Elevation				Velocity			
Scenarios	EC	PCRE	PERC	All	EC	PCRE	PERC	All
RMSE (m or m/s)	0.0027	0.0036	0.0044	0.0037	0.07	0.07	0.06	0.07
MPE (%)	-3.75	8.34	6.18	3.77	15.48	22.5	14.03	17.87

3.1.2 Subsurface Flow

For subsurface flow, the observed pathlines due to dye injection in laboratory experiments (Δ_{wu}/Δ_{bu} =1.84) and the simulated pathlines due to particle tracking in MODPATH for field scale model (Δ_{wu}/Δ_{bu} =7) are presented in Figure 5 to 7. The observed pattern of dye tracks agrees well with simulated particle tracks, such that the following pattern is obtained for EC, PCRE, and PERC scenarios.

For the EC scenario (Figure 5), results showed that when dye was injected in the expansion zone with maximum width, some path lines traveled upstream and some traveled downstream. By injecting dye at the width inflection point downstream from the maximum width location, all path lines converged through the downstream constriction. However, when dye was injected at the width inflection point downstream of the minimum width location, path lines traveled to the upstream constriction. Thus, in the channel with only width undulations fluid particles entered the porous bed from the wider area (high pressure zone) and, after traveling some distance through porous media, returned to free surface flow at the narrower area (low pressure zone). Therefore, fluvial hyporheic flow can be induced with only width undulations, in the absence of bed undulations.

For the PCRE scenario (Figure 6), when dye was injected between the pool trough and downstream riffle crest, the emergence point was near the downstream riffle crest. However, by injecting dye between the trough and the upstream riffle crest, the emergence points would be on the lee side of the upstream riffle. The hyporheic flow in this scenario was driven by hydraulic gradients resulting from both bed and width undulations. Because the upwelling region in this scenario was observed downstream of riffle crest – located in an expansion – the effect of bed undulation on hyporheic flow pattern was greater than the effect of width undulation with Δ_{wu}/Δ_{bu} =1.84.

For the PERC scenario (Figure 7), because the riffle was constricted, the minimum pressure occurred on the riffle crest. This led to the emergence of the dye near the riffle crest, so then free surface flow entered the porous bed from the pool (downwelling) and returned to free surface downstream of the riffle crest (upwelling). Also, for this scenario, the observed hyporheic pathlines are compared with its simulated one in Figure 8, which demonstrated that the numerical model capable to trace the path line for injection points.

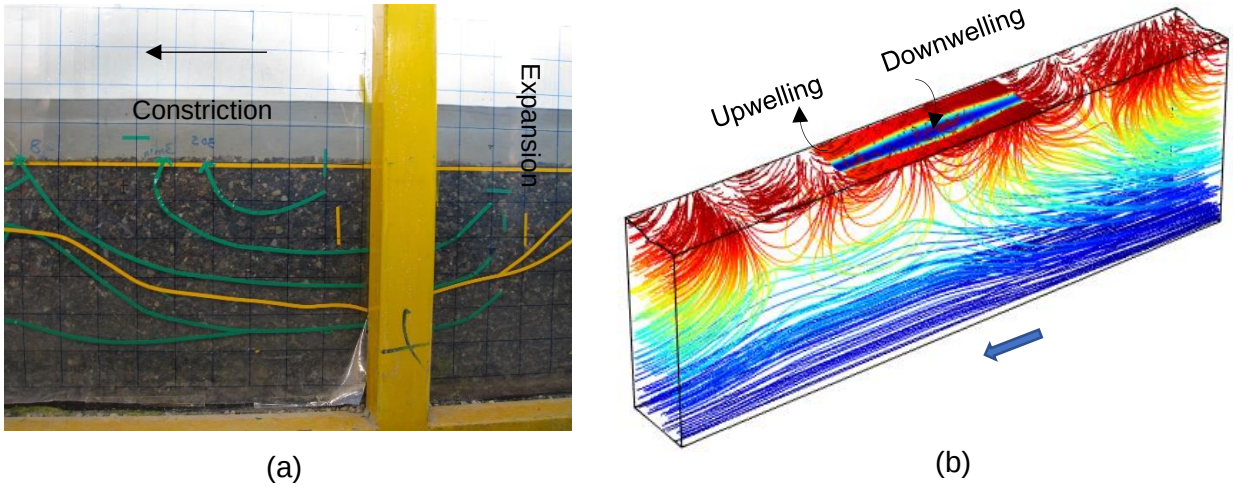

396

397 **Figure 5. The path lines through bed sediment for EC scenario; (a) observed and (b) simulated.**

398

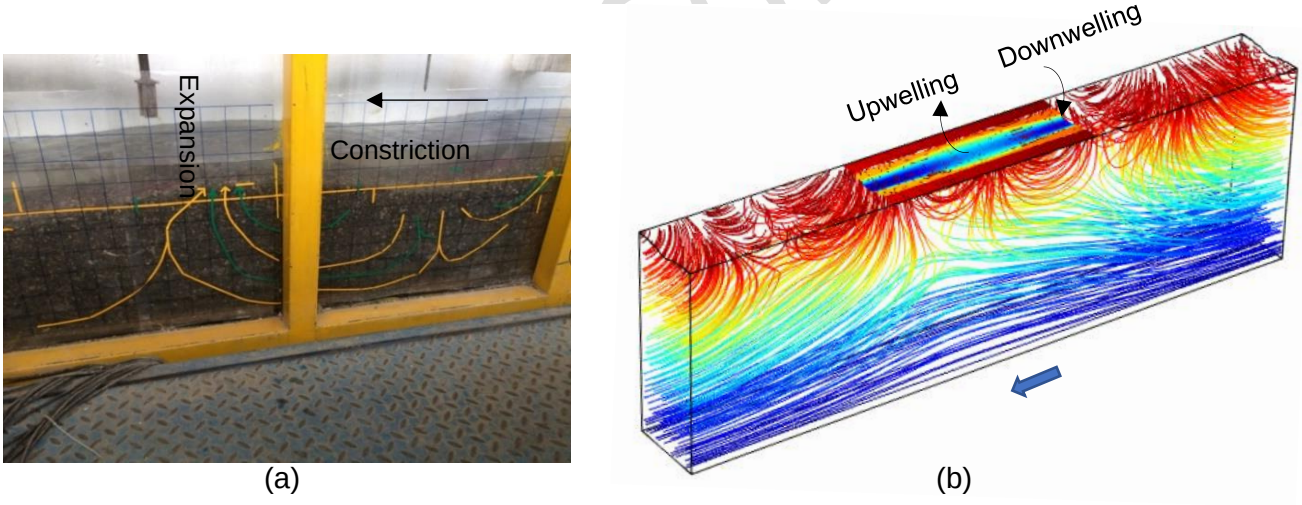

399

400 **Figure 6. The path lines through bed sediment for PCRE scenario; (a) observed and (b) simulated.**

401

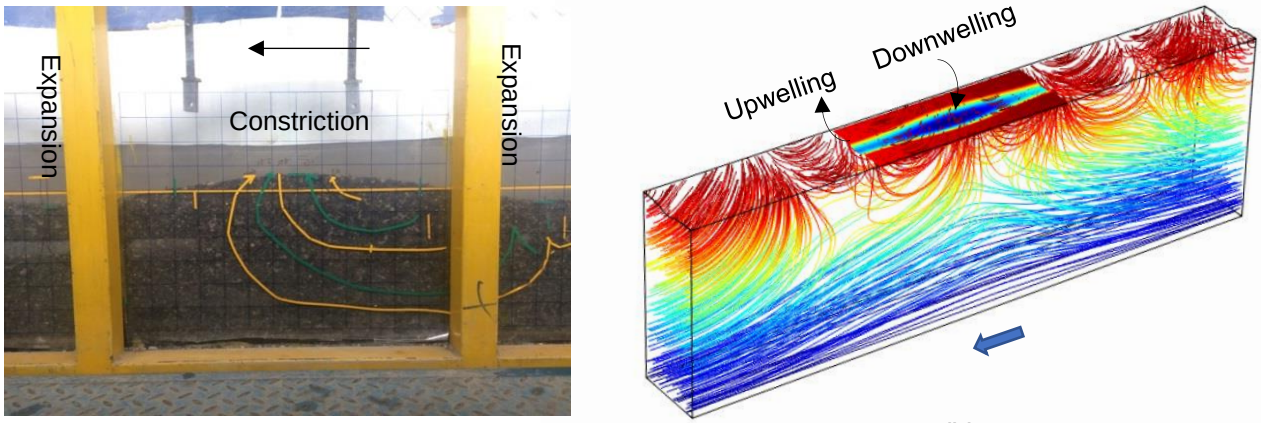

402

403 **Figure 7. The path lines through bed sediment for PERC scenario; (a) observed and (b) simulated.**

404

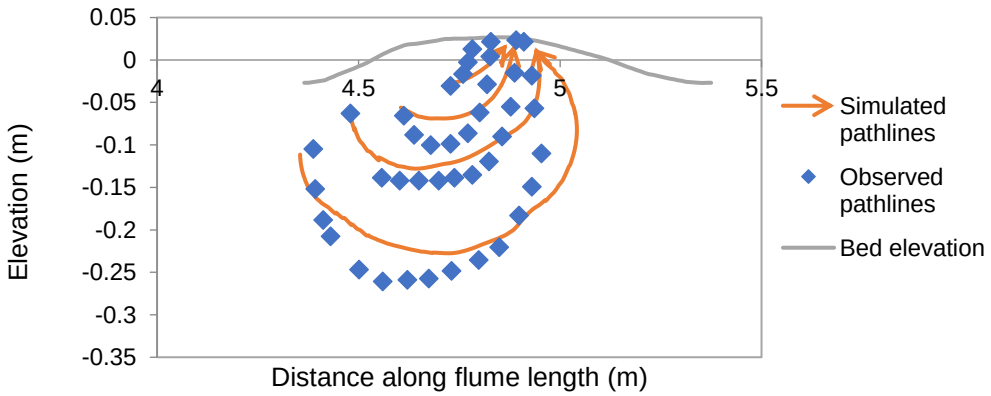

405

406 **Figure 8. Comparison of observed and simulated hyporheic flow path for PERC scenario**

407

408 ## 3.2 Hydraulic Head Distributions at SWI

409 For submerged features (i.e. dune, riffle) the variation of hydraulic head at SWI is a main driver of
410 hyporheic exchanges. Figure 9 and 10 show the plan view of hydraulic head (H) distribution at SWI, for
411 different ratios of Δ_{wu}/Δ_{bu}, for PCRE and PERC scenarios, respectively. The dashed and continuous lines
412 denote the pool and riffle positions, respectively.

413 For PCRE scenarios, by increasing Δ_{wu}/Δ_{bu}, the location of maximum hydraulic head shifted from the width
414 constriction to the width expansion (Figure 9), and also the distance between maximum and minimum

hydraulic head increased. Lateral variations in hydraulic head were observed, with particularly prominent high-pressure zones on the channel edge of the expansion in the PCRE scenario, especially for larger values of Δ_{wu}/Δ_{bu}. Lateral variations in hydraulic head can produce lateral hyporheic flow when the banks are permeable.

For PERC scenarios, of maximum hydraulic head was located at upstream of the riffle and close to the undulated bank and with increasing the ratio of Δ_{wu}/Δ_{bu}, the width of high-pressure zone increased. Because, as Δ_{wu}/Δ_{bu} increased the width of constriction decreased, so the portion of the bank facing the flow increased, thus acted as a barrier and led to the stronger high pressure area behind the minimum constriction width which was in line with the high pressure zone created by riffle (Figure 10). Also, as the ratio of Δ_{wu}/Δ_{bu} increased, the distance between of maximum hydraulic head and of minimum hydraulic head decreased.

For both PERC and PCRE scenarios, the minimum hydraulic head was located at the riffle crest. Also, the longitudinal distance between of maximum hydraulic head and of minimum hydraulic head was longer in PCRE scenarios in comparison with PERC scenarios.

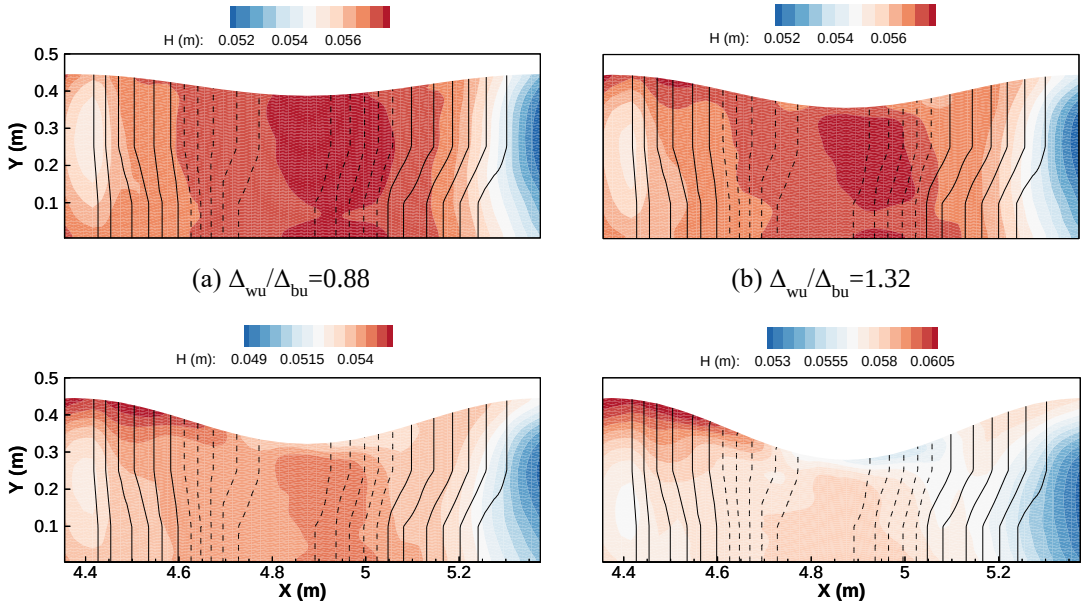

(a) Δ_{wu}/Δ_{bu}=0.88 (b) Δ_{wu}/Δ_{bu}=1.32

(c) Δ_{wu}/Δ_{bu}=1.84 (d) Δ_{wu}/Δ_{bu}=2.5

Figure 9. Simulated hydraulic head distribution for PCRE scenarios for different ratios of Δ_{wu}/Δ_{bu} (flow direction is from left to right).

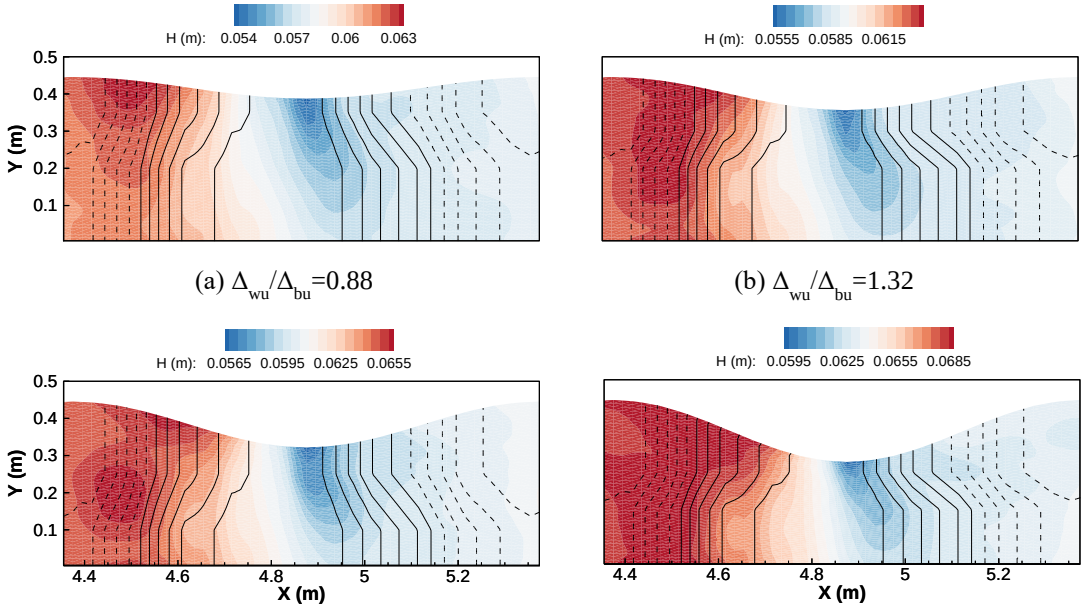

(a) Δ_{wu}/Δ_{bu}=0.88 (b) Δ_{wu}/Δ_{bu}=1.32

(c) Δ_{wu}/Δ_{bu}=1.84 (d) Δ_{wu}/Δ_{bu}=2.5

Figure 10. Simulated hydraulic head distribution for PERC scenarios for different ratios of Δ_{wu}/Δ_{bu} (flow direction is from left to right).

437

438 ### 3.3 Hyporheic Exchange Flow and Residence Time

439 As described in Section 2.4, the hyporheic exchanges and residence time are computed for the particles that
440 enter and subsequently exit the domain only from the streambed. Normalized exchange (Q^*_{HZ}) and
441 normalized median residence time (RT*) are highly sensitive to different ratios of Δ_{wu}/Δ_{bu} (Figure 11 and
442 12).

443 For EC scenarios, as the ratio of Δ_{wu}/Δ_{bu} increased, the Q^*_{HZ} increased and RT* decreased. Because by
444 decreasing the width of the minimum constriction, the average velocity of flow in constriction increased
445 for a given flow discharge. By increasing Δ_{wu}/Δ_{bu}, the contribution of bank undulation on local hydraulic
446 head gradient increased which leads to the higher Q^*_{HZ} and lower RT*.

447 When bedforms were added to width undulations, for both PCRE and PERC scenarios, in comparison to
448 EC scenarios, the normalized hyporheic exchanges increased and normalized residence time decreased (for
449 all ratios of Δ_{wu}/Δ_{bu}). In other words, presence of bedforms enhanced hyporheic exchange. The highest
450 hyporheic exchange was related to the PERC, for which both riffle and width constriction combined to
451 increase the velocity variation through the constriction, so the hydraulic head gradients increased and Q^*_{HZ}
452 increased.

453 For PCRE scenarios, with increasing the ratio of Δ_{wu}/Δ_{bu}, the hydraulic head gradients increased, so Q^*_{HZ}
454 increased and RT* decreased. Also, for PERC scenarios, with increasing this ratio, hyporheic exchanges
455 increased but for the ratio of Δ_{wu}/Δ_{bu} =2.5, as the area which riffle-pool occupied was decreased, the
456 hydraulic head gradient decreased, so the Q^*_{HZ} decreased and RT* increased.

457 By comparing RP and EC scenarios, it can be concluded that bed undulations (RP scenario) led to higher
458 Q^*_{HZ}, except for ratio of Δ_{wu}/Δ_{bu} =2.5, whereas bank undulations (EC scenarios) led to higher median
459 residence time for all modelled channels.

460

461

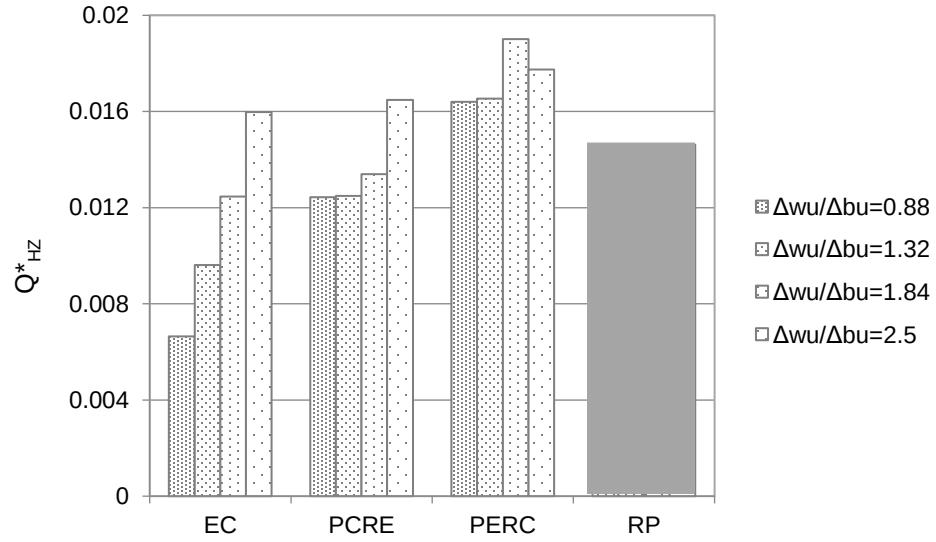

462

463 **Figure 11. Normalized hyporheic exchange for various scenarios and different ratios of Δ_{wu}/Δ_{bu}.**

464

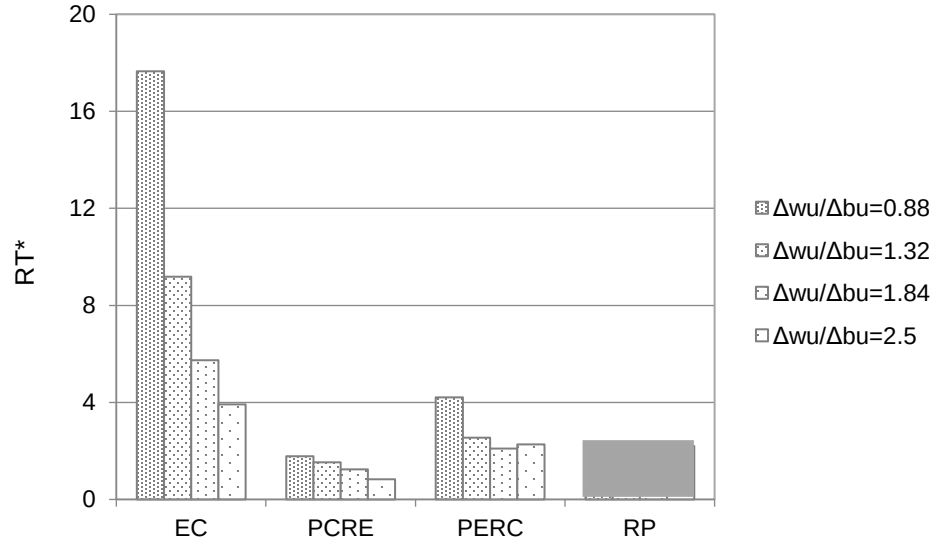

465

466 **Figure 12. Normalized residence time for various scenarios and different ratios of Δ_{wu}/Δ_{bu}.**

467

468 Considering the Brown et al. (2016) models, it was discovered that by adding bed undulations to bank
469 undulations (comparing S2, S4 and S5), Q^*_{HZ} increased and RT* decreased (Table 3). The maximum Q^*_{HZ}
470 occurred when the pool was in the width expansion and riffle in the constriction, which shows the similar
471 behavior to small-scale models. Also, maximum RT* was achieved for the EC scenario.

By adding width undulations to bed undulations (comparing S3, S4 and S5), the RT* increased, whether the riffle was constricted and pool expanded or vice versa. The Q^*_{HZ} for RP and PERC scenarios were similar, which showed that for small amplitude bed form (as here for large scale), the simultaneous effect of bed and width undulations had no significant effect on hyporheic exchanges, when pools were located in width expansions and riffles in width constrictions. Hyporheic exchange and residence time was much more sensitive to variations in width amplitude in the absence of bed undulations.

Table 3. Normalized hyporheic exchange (Q^*_{HZ}) and residence time (RT*) for different models of Brown et al. (2016)

River type	Q^*_{HZ}	RT*
S2	0.003555	81.44
S3	0.010067	23.47
S4	0.007594	35.26
S5	0.010345	42.83

3.4 Residence Time Distribution

Histograms of residence time distributions (RTD) and fitted log-normal curves are plotted in Figure 13, for PCRE and PERC scenarios. For PCRE scenarios, all ratios of Δ_{wu}/Δ_{bu} are well distributed with a log-normal distribution. For all ratios of Δ_{wu}/Δ_{bu} the skewness is positive which means the number of path lines with long residence time is low, and as Δ_{wu}/Δ_{bu} increased, the distributions become close to the symmetrical. For PERC scenarios, a bimodal distribution was observed with two peaks. The fitted log-normal curve also proposed by other investigations for only riffle-pool sequences (Tonina and Buffington 2007, Trauth et al. 2013).

Histograms of residence time distributions for large scale models are also log-normally distributed (Figure 14), but they show a negative skewness which means that the number of particles with long residence time is high.

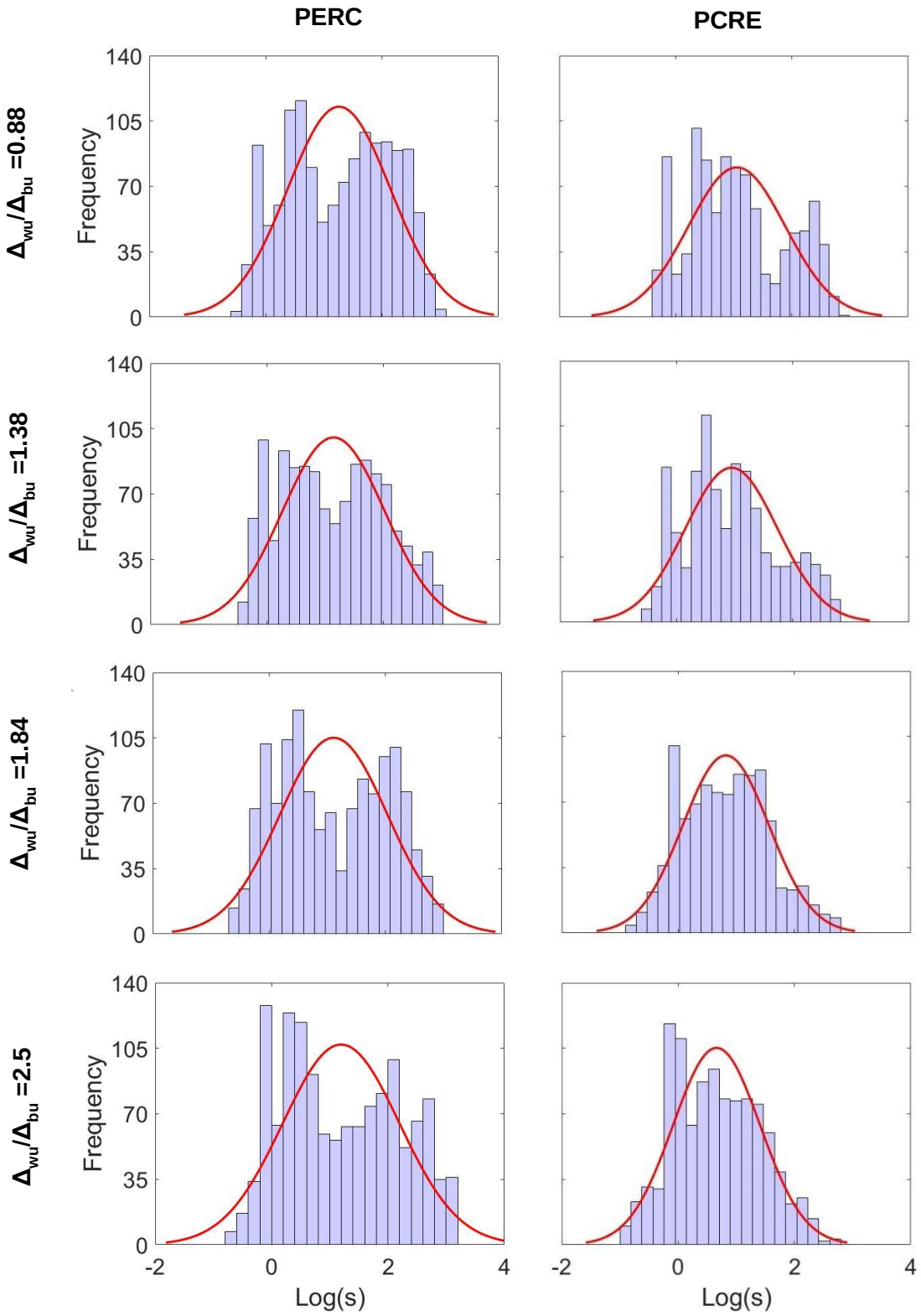

Figure 13. Residence time distribution for PCRE and PERC scenarios, for different ratios of Δ_{wu}/Δ_{bu}.

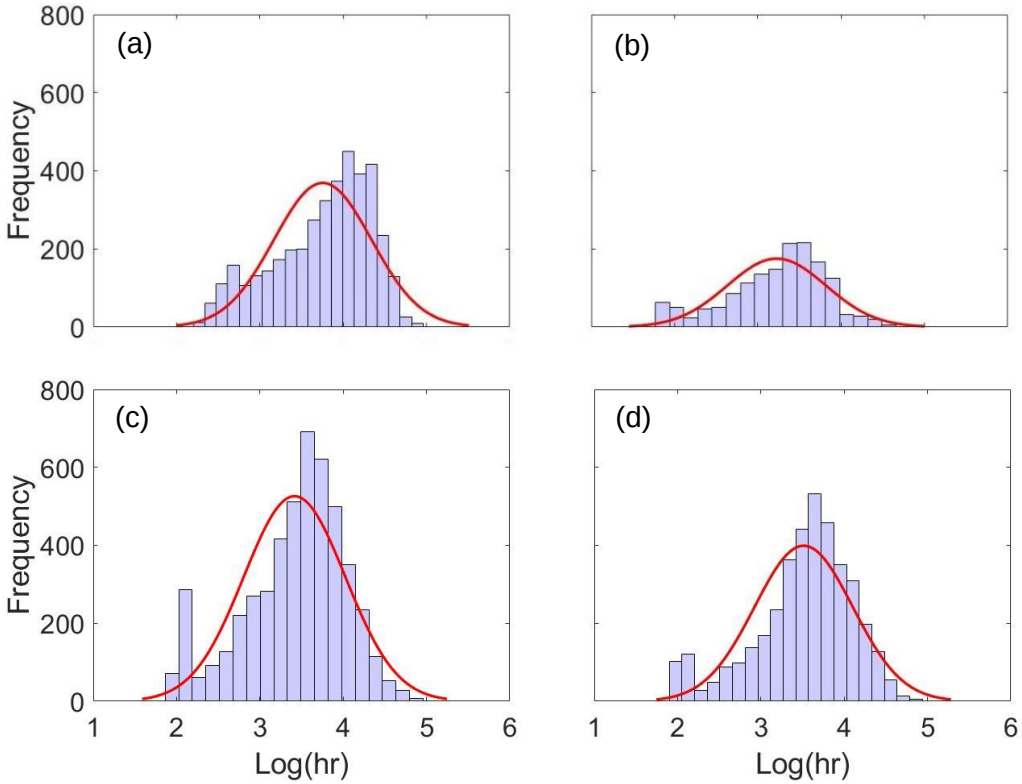

498

499 **Figure 14. Histograms of residence time distributions (RTD) and their fitted normal curves for Brown et al.**
500 **(2016) configurations, at Q=125 m3/s for, (a) S2, (b) S3, (c) S4, and (d) S5.**

501

502 ## 3.5 Traveling Distance

503 Due to the hydraulic head gradients that occurred laterally across the flume, path lines also deviated in
504 lateral direction. The results showed that for EC scenarios, the median lateral travel distance was always
505 less the 80% of the median longitudinal travel distance and as the constriction width decreased (higher ratio
506 of the Δ_{wu}/Δ_{bu}), the median longitudinal and median lateral travel distances decreased.

507 For PCRE scenarios, the hydraulic head gradient across the flume was higher than PERC scenarios and
508 lead to the longer median lateral travel distance which increased with Δ_{wu}/Δ_{bu}. But for PERC scenarios, the
509 hydraulic head distribution along channel width was more uniform in comparison with PCRE scenarios and
510 led to the shorter median lateral travel distance. Also, as Δ_{wu}/Δ_{bu} increased the hydraulic head distribution
511 become more uniform and lead to the shorter median lateral travel distance.

512

3.6 Hyporheic Exchanges Depth

For PCRE and PERC scenarios, by average 93 percent of total exchange is transported by path lines within 20 cm below the mean bed form amplitude (i.e. 58.8 percent of subsurface layer thickness) and as the ratio of Δ_{wu}/Δ_{bu} decreased, the hyporheic exchange depth increased. For bed form only scenario, Tonina and Buffington (2011) indicated that in order to make sure that the depth of sediment layer did not affect hyporheic exchanges, this depth should be more than one third of the wavelength. But our results showed that for both bed and bank undulation scenarios, the depth of sediment layer could be less than this criterion and further experiments are warranted to define a new criterion. Also, the maximum exchange depth for PERC scenarios were less than PCRE scenarios.

4. Discussion

4.1 Non-uniform channel pattern

Bed undulations were the focus of early geomorphic research into riffle-pool morphology (Figure 15a) (e.g., Keller 1971, Milne 1982, Richards 1976b). While datasets show wide scatter in channel width (Figure 15b) (e.g., Keller and Melhorn 1978, Xu 2004) – scatter that might signal important underlying patterns and processes – that has largely been overlooked in favor of relating metrics of morphological central tendency to each other and to simplified process regimes (e.g., Bieger et al. 2015, Osterkamp et al. 1983). Exceptions certainly exist (e.g., Merritt and Wohl 2003, Richards 1976a, Stewardson 2005, Trainor and Church 2003). Today, widespread availability of meter-resolution digital elevation models of rivers enables a fresh, deeper look at patterns of topographic variability (Scown et al. 2015) and the processes they contribute to (Strom et al. 2016, Wyrick and Pasternack 2016). River classifications and scientific studies are increasingly embracing new fluvial metrics of geometric variability (e.g., Byrne et al. 2020, Pasternack et al. 2018a, Wohl 2016), leading to a greater understanding of the scope of variability in rivers, the typical patterns in different settings, and the environmental roles variability play.

Individual river reaches exhibit a wide range of values for depth and width variability metrics (Byrne et al. 2020, Laub et al. 2012), but there are two common endmembers associated with distinct valley settings: PCRE and PERC (Figure 15c and Figure 15d, respectively). The PERC configuration with nozzles and oversized units is widespread in mountains due to two regimes. First, coarse bedload in canyon-confined bedrock rivers can scour out deep, wide pools between steep, confined, shallow units (riffles, rapids, steps, and slides). Second, small, steep tributaries to wider mountain canyons can deliver sufficient coarse sediment to constrict a canyon to a small fraction of its width. PERC reaches can also occur naturally in small headland meadows and lowland valley streams due to local (wood and boulder) obstructions and

resistant hardpans forming nozzles. In engineering practice, the PERC configuration has come to dominate in whitewater park design (Kolden et al. 2016) and a type of channel restoration called "regenerative stormwater conveyance (Duan et al. 2019). The latter is especially intended to drive hyporheic flow, potentially enhancing denitrification in streams degraded by anthropogenic high nutrient loads (Craig et al. 2008, Klocker et al. 2009, Merill and Tonjes 2014, Tuttle et al. 2014).

The PCRE configuration with wide bar and constricted pool units is naturally widespread in partially confined to unconfined valleys with alluvial, self-formed channels and riverbed slopes of 0.001 to 0.02. In the absence of fixed obstructions, it is thought to be self-maintaining due to energy minimization, flow convergence routing, and grain size differentiation between units (Bayat et al. 2017, MacWilliams Jr et al. 2006, Yang 1971). Mindful design of PCRE is limited as of yet, but advocated by academics due to its self-sustainability based on flume, field, and numerical modeling studies (e.g., Jackson et al. 2015, Repetto and Tubino 2001, Wheaton et al. 2010). While studies have investigated hyporheic and denitrification effects in reaches with constructed riffles and pools (Mendoza-Lera and Datry 2017, Merill and Tonjes 2014, Rivers et al. 2018), care has not been taken to isolate the PCRE configuration. Overall, both PERC and PCRE configurations are widespread in nature and increasingly used in river engineering, warranting a better understanding of their hyporheic flow processes.

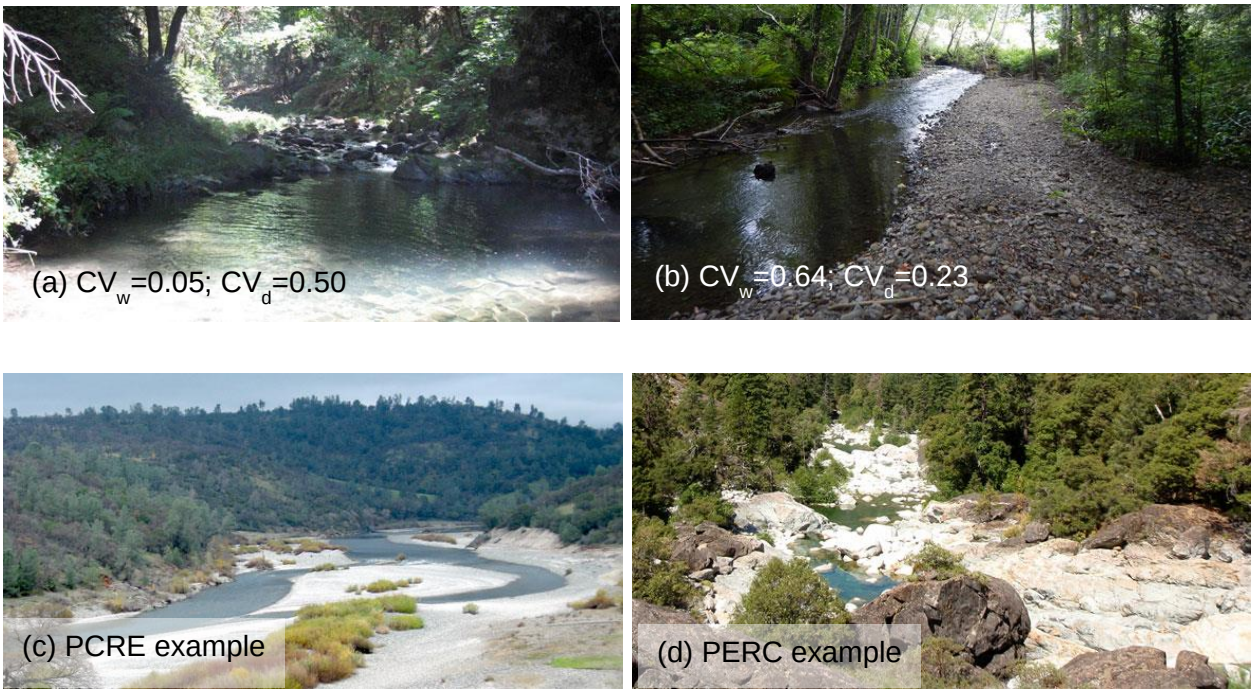

Figure 15. Rivers in California exhibiting the four different undulation patters addressed in this study: (a) bed undulating, (b) width undulating, (c) bed and width undulations positively correlated (PCRE), and (d)

bed and width undulations negatively correlated (PERC). For (a) and (b), coefficient of variation (CV) metrics for width and depth are shown

4.2 Hyporheic response to channel non-uniformity

In this study, for the first time we present the hydraulic head distribution along systematically varying channel bed and width undulations, including those linked with two different phase angles commonly observed in nature. The location of maximum and minimum hydraulic head distribution depends on bed or width amplitude. Our results show that for EC (supplementary Figure 1) and PERC (Figure 10) scenarios the pattern of hydraulic head distributions does not change a lot for various ratios of Δ_{wu}/Δ_{bu}. But, for PCRE scenarios the location of minimum and maximum hydraulic head change for higher ratios of Δ_{wu}/Δ_{bu}.

Investigation of near bed velocities at different positions of pool trough and riffle crest along channel width reveal that for ratios of Δ_{wu}/Δ_{bu} =1.84, 2.5, the near bed velocities at distances near to the sinusoidal width, are higher for pool in the narrowest width than riffle in the widest width. So, it can be concluded that not only flow discharge (mentioned by previous studies), but also ratio of width undulation amplitude to bed undulation amplitude has an effect on the velocity reversal hypothesis. However, for PERC scenarios, no reversal velocity was observed because according to the energy principle in subcritical flow, constricting a riffle leads to higher velocities there than ate the pool. Further investigations are recommended to investigate the effect of reversal velocity on hyporheic exchanges under various ratios of Δ_{wu}/Δ_{bu} and flow conditions.

As mentioned in the introduction section, Buffington and Tonina (2009) stated that one of the mechanisms causing hyporheic exchange is spatial changes in alluvial area (alluvial depth or the valley width). For EC scenarios, we find that the path lines are downwelled in expansion areas and upwelled in constriction areas which is in line with their findings. In their 2011 paper, they discussed about the effect of alluvial depth on HE, but in this paper, we investigate the effect of alluvial width (EC scenarios) and we find that as the alluvial width decrease (higher width amplitude), the Q^*_{HZ} increase and RT* decrease.

For PCRE scenarios, the Q^*_{HZ} increased with Δ_{wu}/Δ_{bu}, but for PERC scenarios, with increasing this ratio, Q^*_{HZ} increased up to Δ_{wu}/Δ_{bu} =1.84 but then decreased for Δ_{wu}/Δ_{bu} =2.5. It seemed that for PERC scenario, according to the energy principle, the ratio of Δ_{wu}/Δ_{bu} =2.5 was near to the choking condition. This scenario associated with the nozzle effect, which high velocity and low pressure after riffle crest, can be led to the choking condition.

Comparing EC scenarios with PCRE and PERC show that the simultaneous effects bed and width undulations lead to the higher Q^*_{HZ} due to the higher hydraulic head gradients which correspond to the lower RT*, and is in line with the results of most of the hyporheic studies; which showed higher Q_{HZ} with lower residence time and vice versa (Tonina and Buffington 2011, Trauth et al. 2013). But comparison between PERC and PCRE scenarios reveal that however the PERC scenarios show higher Q^*_{HZ}, but they don't produce lower RT due to longer flow paths.

Stonedahl et al. (2013) for various ratio of meander sinusitis showed that presence of dune at meanders led to the higher HE in comparison to the only meander cases. Our results also demonstrate that HE increases as bed undulations are added to width undulations.

In order to extend the results for large scale cases in rivers, the configurations studied by Brown et al. (2016), for investigating bed shear stress along the sequences of expansion-constriction widths, with riffle-pool sequences and also with flat bed, were examined numerically. Due to this fact that the application of 3D models for field-scale simulations is computationally expensive, SRH-2D model, which solved the depth-averaged St. Venant equations was used to simulate free surface flow characteristics for scenarios S2, S3, S4 and S5. To extend the research methodology to rivers, a 2D surface flow simulation model can be run to calculate hydraulic head at SWI, which needs less input parameters to calibrate the model and is less expensive in compare with 3D CFD models. After calculation of hydraulic head, the flow through porous media can be determined by assigning the calculated hydraulic head as a Dirichlet boundary at SWI and computing the hyporheic zone characteristics.

The results of field scale scenarios show that there is good agreement with experimental and numerical simulation scenarios in terms of variations of Q^*_{HZ} and RT*. As demonstrated in Table 2, the ratio of Δ_{wu}/Δ_{bu} are not identical for both large (field) and small-scale cases. For field cases the amplitude of width undulation is much more than bed undulation and for small scale cases we have some case with $\Delta_{wu}/\Delta_{bu} >1$ and some cases with $\Delta_{wu}/\Delta_{bu} <1$. For both of these two scales, the simultaneous effect of channel bed and width undulations reveal that maximum Q^*_{HZ} achieve when pool is located in expansion and riffle in constriction, as both constriction and shallowness converge flow in the same way. The residence time distribution for field scale scenarios shows log-normally distributed with negative skewness which is due to high frequency of longer and deeper path lines. Further investigations are needed to specifically determine whether bed amplitude is more effective in HE or width amplitude. The results of this study showed for all scenarios, the residence time can well represented by log-normal distribution which also proposed in literature (Tonina and Buffington 2007, Trauth et al. 2013).

5. Conclusion

In this paper, a series of laboratory experiments and numerical simulations were done to investigate the effect of channel width undulation and also simultaneous effect of channel bed and width undulations on hyporheic exchanges. The OpenFOAM and MODFLOW software were applied for surface water and subsurface water simulations, respectively. Also, the particle tracking method in MODPATH was used to derive hyporheic zone characteristics.

The laboratory observations and also numerical simulations showed that at least for the geometric conditions of this study, the location of the upwelling hyporheic flow paths depends on the location of riffle crest rather than the location of riffle crest relative to the sinusoidal banks.

We found that for EC scenarios, the normalized hyporheic exchanges (Q^*_{ex}) increased with Δ_{wu}/Δ_{bu}, while normalized median residence time (RT*) decreased. We also found that, by adding bed forms to the bank undulations, the Q^*_{ex} increased and RT* decreased, for a given Δ_{wu}/Δ_{bu}. For PCRE scenarios, the Q^*_{ex} increased with Δ_{wu}/Δ_{bu}, while RT* decreased. But for PERC scenarios, the Q^*_{ex} increased with Δ_{wu}/Δ_{bu} until the ratio of Δ_{wu}/Δ_{bu} =1.84, and then decreased for Δ_{wu}/Δ_{bu} =2.5. From the hydraulic point of view, it seems that this ratio is a threshold for starting choking conditions. Further investigations are needed to determine on which ratio between bank and bed amplitude, these conditions occur and the effect of one of them dominated by the other one.

Our results demonstrated that for both small scale and large-scale models, the only width undulations scenarios have longest residence time, and the scenarios which pool located in expansion and riffle in constriction had the highest hyporheic exchange. The findings of this study will be applicable for river restoration projects. In General, in rivers which have width undulations, constructing artificial riffle-pool sequences, in both positions (PCRE or PERC), lead to the higher hyporheic exchanges which would be beneficial for the project aiming to intensify oxygen rate for microorganism living in the streambed. However, by artificially construction of pool in expansion areas and riffle in constriction areas, the maximum Q^*_{ex} and RT* will be occur.

In this study the channel bank was assumed rigid and laterally hyporheic flow was ignored, so effect of porous bank on hyporheic flow characteristics is proposed for future study. Also, construction of pool in expansion areas and riffle in contraction areas of rivers may develop the secondary currents in rivers. So, 3D velocity measurement to assess the secondary flow and the rule of turbulence on HE characteristics should be addressed in future works.

Acknowledgment

The authors would like to acknowledge Department of Infrastructure Engineering at The University of Melbourne for providing the facility as sabbatical for second author and Department of Hydrogeology of Helmholtz Center for Environmental Research—UFZ in Leipzig, especially Prof. Jan H. Fleckenstein for hosting first author as guest researcher to doing the numerical simulations in this center. The financial support of this research was provided by Ministry of Science, Research and Technology of Iran. The contribution of Michael Stewardson to this research was supported by Australian Research Council Grant DP130103619. The contribution of Gregory Pasternack to this research was supported by the USDA National Institute of Food and Agriculture, Hatch project number CA-D-LAW-7034-H.

References.

Balbarini, N., Boon, W.M., Nicolajsen, E., Nordbotten, J.M., Bjerg, P.L. and Binning, P.J. (2017) A 3-D numerical model of the influence of meanders on groundwater discharge to a gaining stream in an unconfined sandy aquifer. Journal of Hydrology 552, 168-181. https://doi.org/10.1016/j.jhydrol.2017.06.042

Battin, T.J., Kaplan, L.A., Findlay, S., Hopkinson, C.S., Marti, E., Packman, A.I., Newbold, J.D. and Sabater, F. (2008) Biophysical controls on organic carbon fluxes in fluvial networks. Nature geoscience 1(2), 95. https://doi.org/10.1038/ngeo101

Bayat, E., Rodríguez, J.F., Saco, P.M., de Almeida, G.A., Vahidi, E. and García, M.H. (2017) A tale of two riffles: Using multidimensional, multifractional, time-varying sediment transport to assess self-maintenance in pool-riffle sequences. Water Resources Research 53(3), 2095-2113. https://doi.org/10.1002/2016WR019464

Bencala, K.E. (2000) Hyporheic zone hydrological processes. Hydrological Processes 14(15), 2797-2798.

Bieger, K., Rathjens, H., Allen, P.M. and Arnold, J.G. (2015) Development and evaluation of bankfull hydraulic geometry relationships for the physiographic regions of the United States. JAWRA Journal of the American Water Resources Association 51(3), 842-858. https://doi.org/10.1111/jawr.12282

Bittner, L.D. (1994) River bed response to channel width variation: Theory and experiments, University of Illinois at Urbana-Champaign, Illinois, United States.

683 Boano, F., Camporeale, C., Revelli, R. and Ridolfi, L. (2006) Sinuosity-driven hyporheic exchange in
684 meandering rivers. Geophysical Research Letters 33(18). https://doi.org/10.1029/2006GL027630

685 Boulton, A.J., Findlay, S., Marmonier, P., Stanley, E.H. and Valett, H.M. (1998) The functional
686 significance of the hyporheic zone in streams and rivers. Annual Review of Ecology and Systematics 29(1),
687 59-81. https://doi.org/10.1146/annurev.ecolsys.29.1.59

688 Brown, R.A. and Pasternack, G.B. (2019) How to build a digital river. Earth-Science Reviews.
689 https://doi.org/10.1016/j.earscirev.2019.04.028

690 Brown, R.A., Pasternack, G.B. and Lin, T. (2016) The topographic design of river channels for form-
691 process linkages. Environmental management 57(4), 929-942. https://doi.org/10.1007/s00267-015-0648-0

692 Brown, R.A., Pasternack, G.B. and Wallender, W.W. (2014) Synthetic river valleys: Creating prescribed
693 topography for form–process inquiry and river rehabilitation design. Geomorphology 214, 40-55.
694 https://doi.org/10.1016/j.geomorph.2014.02.025

695 Buckrell, E. (2017) The formation and adjustment of a pool-riffle sequence in a gravel bed flume,
696 University of British Columbia.

697 Buffington, J.M. and Montgomery, D.R. (1999) Effects of hydraulic roughness on surface textures of
698 gravel-bed rivers. Water Resources Research 35(11), 3507-3521. https://doi.org/10.1029/1999WR900138

699 Buffington, J.M. and Tonina, D. (2009) Hyporheic exchange in mountain rivers II: effects of channel
700 morphology on mechanics, scales, and rates of exchange. Geography Compass 3(3), 1038-1062.
701 https://doi.org/10.1111/j.1749-8198.2009.00225.x

702 Byrne, C.F., Pasternack, G.B., Guillon, H., Lane, B.A. and Sandoval-Solis, S. (2020) Reach-scale bankfull
703 channel types can exist independently of catchment hydrology. Earth Surface Processes and Landforms.
704 https://doi.org/10.1002/esp.4874

705 Caamaño, D., Goodwin, P., Buffington, J.M., Liou, J.C. and Daley-Laursen, S. (2009) Unifying criterion
706 for the velocity reversal hypothesis in gravel-bed rivers. Journal of Hydraulic Engineering 135(1), 66-70.
707 https://doi.org/10.1061/(ASCE)0733-9429(2009)135:1(66)

708 Cardenas, M.B. (2009a) A model for lateral hyporheic flow based on valley slope and channel sinuosity.
709 Water Resources Research 45(1). https://doi.org/10.1029/2008WR007442

710 Cardenas, M.B. (2009b) Stream-aquifer interactions and hyporheic exchange in gaining and losing sinuous
711 streams. Water Resources Research 45(6). https://doi.org/10.1029/2008WR007651

712 Cheng, N.-S. and Chiew, Y.-M. (1998) Modified logarithmic law for velocity distribution subjected to
713 upward seepage. Journal of Hydraulic Engineering 124(12), 1235-1241.
714 https://doi.org/10.1061/(ASCE)0733-9429(1998)124:12(1235)

715 Craig, L.S., Palmer, M.A., Richardson, D.C., Filoso, S., Bernhardt, E.S., Bledsoe, B.P., Doyle, M.W.,
716 Groffman, P.M., Hassett, B.A. and Kaushal, S.S. (2008) Stream restoration strategies for reducing river
717 nitrogen loads. Frontiers in Ecology and the Environment 6(10), 529-538. https://doi.org/10.1890/070080

718 De Almeida, G.A.M. and Rodríguez, J.F. (2011) Understanding pool-riffle dynamics through continuous
719 morphological simulations. Water Resources Research 47(1). https://doi.org/10.1029/2010WR009170

720 De Almeida, G.A.M. and Rodríguez, J.F. (2012) Spontaneous formation and degradation of pool-riffle
721 morphology and sediment sorting using a simple fractional transport model. Geophysical Research Letters
722 39(6). https://doi.org/10.1029/2012GL051059

723 Duan, S., Mayer, P.M., Kaushal, S.S., Wessel, B.M. and Johnson, T. (2019) Regenerative stormwater
724 conveyance (RSC) for reducing nutrients in urban stormwater runoff depends upon carbon quantity and
725 quality. Science of the Total Environment 652, 134-146. https://doi.org/10.1016/j.scitotenv.2018.10.197

726 Emery, J.C., Gurnell, A.M., Clifford, N.J., Petts, G.E., Morrissey, I.P. and Soar, P.J. (2003) Classifying the
727 hydraulic performance of riffle–pool bedforms for habitat assessment and river rehabilitation design. River
728 Research and Applications 19(5-6), 533-549. https://doi.org/10.1002/rra.744

729 Farshi, F., Kabiri-Samani, A., Chamani, M.R. and Atoof, H. (2018) Evaluation of the Secondary Current
730 Parameter and Depth-Averaged Velocity in Curved Compound Open Channels. Journal of Hydraulic
731 Engineering 144(9), 04018059.

732 Fehlman, H.M. (1985) Resistance components and velocity distributions of open channel flows over
733 bedforms, Colorado State University, Fort Collins, United States.

734 Gariglio, F.P., Tonina, D. and Luce, C.H. (2013) Spatiotemporal variability of hyporheic exchange through
735 a pool-riffle-pool sequence. Water Resources Research 49(11), 7185-7204.
736 https://doi.org/10.1002/wrcr.20419

737 Gomez-Velez, J., Wilson, J., Cardenas, M. and Harvey, J. (2017) Flow and residence times of dynamic
738 river bank storage and sinuosity-driven hyporheic exchange. Water Resources Research 53(10), 8572-8595.
739 https://doi.org/10.1002/2017WR021362

740 Greenshields, C.J. (2015) OpenFOAM: The Open Source CFD Toolbox, User Guide. OpenFOAM
741 Foundation Ltd.

742 Han, B. and Endreny, T.A. (2014) Detailed river stage mapping and head gradient analysis during meander
743 cutoff in a laboratory river. Water Resources Research 50(2), 1689-1703.

744 Jackson, J.R., Pasternack, G.B. and Wheaton, J.M. (2015) Virtual manipulation of topography to test
745 potential pool–riffle maintenance mechanisms. Geomorphology 228, 617-627.
746 https://doi.org/10.1016/j.geomorph.2014.10.016

747 Jacobson, R.B. and Gran, K.B. (1999) Gravel sediment routing from widespread, low-intensity landscape
748 disturbance, Current River Basin, Missouri. Earth Surface Processes and Landforms: The Journal of the
749 British Geomorphological Research Group 24(10), 897-917. https://doi.org/10.1002/(SICI)1096-
750 9837(199909)24:10<897::AID-ESP18>3.0.CO;2-6

751 Jellesma, M. (2013) Form drag of subaqueous dune configurations, University of Twente.

752 Keller, E. and Melhorn, W. (1978) Rhythmic spacing and origin of pools and riffles. Geological Society of
753 America Bulletin 89(5), 723-730. https://doi.org/10.1130/0016-7606(1978)89<723:RSAOOP>2.0.CO;2

754 Keller, E.A. (1971) Areal sorting of bed-load material: the hypothesis of velocity reversal.

755 Klocker, C.A., Kaushal, S.S., Groffman, P.M., Mayer, P.M. and Morgan, R.P. (2009) Nitrogen uptake and
756 denitrification in restored and unrestored streams in urban Maryland, USA. Aquatic Sciences 71(4), 411-
757 424. https://doi.org/10.1007/s00027-009-0118-y

758 Kolden, E., Fox, B., Bledsoe, B. and Kondratieff, M. (2016) Modelling whitewater park hydraulics and fish
759 habitat in Colorado. River Research and Applications 32(5), 1116-1127. https://doi.org/10.1002/rra.2931

760 Lane, B.A., Pasternack, G.B. and Sandoval Solis, S. (2018) Integrated analysis of flow, form, and function
761 for river management and design testing. Ecohydrology 11(5), e1969. https://doi.org/10.1002/eco.1969

762 Laub, B.G., Baker, D.W., Bledsoe, B.P. and Palmer, M.A. (2012) Range of variability of channel
763 complexity in urban, restored and forested reference streams. Freshwater Biology 57(5), 1076-1095.
764 https://doi.org/10.1111/j.1365-2427.2012.02763.x

765 MacWilliams Jr, M.L., Wheaton, J.M., Pasternack, G.B., Street, R.L. and Kitanidis, P.K. (2006) Flow
766 convergence routing hypothesis for pool-riffle maintenance in alluvial rivers. Water Resources Research
767 42(10). https://doi.org/10.1029/2005WR004391

768 McDonald, M.G. and Harbaugh, A.W. (1988) A modular three-dimensional finite-difference ground-water
769 flow model, US Geological Survey Reston, VA. https://doi.org/10.3133/twri06A1

770 Mendoza-Lera, C. and Datry, T. (2017) Relating hydraulic conductivity and hyporheic zone
771 biogeochemical processing to conserve and restore river ecosystem services. Science of the Total
772 Environment 579, 1815-1821. https://doi.org/10.1016/j.scitotenv.2016.11.166

773 Merill, L. and Tonjes, D.J. (2014) A review of the hyporheic zone, stream restoration, and means to enhance
774 denitrification. Critical Reviews in Environmental Science and Technology 44(21), 2337-2379.
775 https://doi.org/10.1080/10643389.2013.829769

776 Merritt, D.M. and Wohl, E.E. (2003) Downstream hydraulic geometry and channel adjustment during a
777 flood along an ephemeral, arid-region drainage. Geomorphology 52(3-4), 165-180.
778 https://doi.org/10.1016/S0169-555X(02)00241-6

779 Milne, J. (1982) Bed-material size and the riffle-pool sequence. Sedimentology 29(2), 267-278.
780 https://doi.org/10.1111/j.1365-3091.1982.tb01723.x

781 Montgomery, D.R., Buffington, J.M., Smith, R.D., Schmidt, K.M. and Pess, G. (1995) Pool spacing in
782 forest channels. Water Resources Research 31(4), 1097-1105. https://doi.org/10.1029/94WR03285

783 Nelson, P.A., Brew, A.K. and Morgan, J.A. (2015) Morphodynamic response of a variable-width channel
784 to changes in sediment supply. Water Resources Research 51(7), 5717-5734.
785 https://doi.org/10.1002/2014WR016806

786 Osterkamp, W., Lane, L.J. and Foster, G. (1983) An analytical treatment of channel-morphology relations,
787 US Government Printing Office.

788 Pasternack, G.B., Baig, D., Weber, M.D. and Brown, R.A. (2018a) Hierarchically nested river landform
789 sequences. Part 1: Theory. Earth Surface Processes and Landforms 43(12), 2510-2518.
790 https://doi.org/10.1002/esp.4411

791 Pasternack, G.B., Baig, D., Weber, M.D. and Brown, R.A. (2018b) Hierarchically nested river landform
792 sequences. Part 2: Bankfull channel morphodynamics governed by valley nesting structure. Earth Surface
793 Processes and Landforms 43(12), 2519-2532. https://doi.org/10.1002/esp.4410

794 Pasternack, G.B., Bounrisavong, M.K. and Parikh, K.K. (2008) Backwater control on riffle–pool
795 hydraulics, fish habitat quality, and sediment transport regime in gravel-bed rivers. Journal of Hydrology
796 357(1-2), 125-139. https://doi.org/10.1016/j.jhydrol.2008.05.014

797 Pescimoro, E., Boano, F., Sawyer, A.H. and Soltanian, M.R. (2019) Modeling influence of sediment
798 heterogeneity on nutrient cycling in streambeds. Water Resources Research 55(5), 4082-4095.
799 https://doi.org/10.1029/2018WR024221

800 Peterson, E.W. and Sickbert, T.B. (2006) Stream water bypass through a meander neck, laterally extending
801 the hyporheic zone. Hydrogeology Journal 14(8), 1443-1451. https://doi.org/10.1007/s10040-006-0050-3

802 Prinos, P. (1995) Bed-suction effects on structure of turbulent open-channel flow. Journal of Hydraulic
803 Engineering 121(5), 404-412. https://doi.org/10.1061/(ASCE)0733-9429(1995)121:5(404)

804 Repetto, R. and Tubino, M. (2001) Topographic expressions of bars in channels with variable width.
805 Physics and Chemistry of the Earth, Part B: Hydrology, Oceans and Atmosphere 26(1), 71-76.
806 https://doi.org/10.1016/S1464-1909(01)85017-6

807 Repetto, R., Tubino, M. and Paola, C. (2002) Planimetric instability of channels with variable width. Journal
808 of Fluid Mechanics 457, 79-109. https://doi.org/10.1017/S0022112001007595

809 Revelli, R., Boano, F., Camporeale, C. and Ridolfi, L. (2008) Intra-meander hyporheic flow in alluvial
810 rivers. Water Resources Research 44(12). https://doi.org/10.1029/2008WR007081

811 Richards, K. (1976a) Channel width and the riffle-pool sequence. Geological Society of America Bulletin
812 87(6), 883-890. https://doi.org/10.1130/0016-7606(1976)87<883:CWATRS>2.0.CO;2

813 Richards, K. (1976b) The morphology of riffle-pool sequences. Earth Surface Processes 1(1), 71-88.
814 https://doi.org/10.1002/esp.3290010108

Rivers, E.N., McMillan, S.K., Bell, C.D. and Clinton, S.M. (2018) Effects of urban stormwater control measures on denitrification in receiving streams. Water 10(11), 1582. https://doi.org/10.3390/w10111582

Schwartz, J.S. and Herricks, E.E. (2007) Evaluation of pool-riffle naturalization structures on habitat complexity and the fish community in an urban Illinois stream. River Research and Applications 23(4), 451-466. https://doi.org/10.1002/rra.986

Schwartz, J.S., Neff, K.J., Dworak, F.E. and Woockman, R.R. (2015) Restoring riffle-pool structure in an incised, straightened urban stream channel using an ecohydraulic modeling approach. Ecological Engineering 78, 112-126. https://doi.org/10.1016/j.ecoleng.2014.06.002

Schwindt, S., Larrieu, K., Pasternack, G.B. and Rabone, G. (2020) River Architect. SoftwareX 11, 100438. https://doi.org/10.1016/j.softx.2020.100438

Scown, M.W., Thoms, M.C. and De Jager, N.R. (2015) Floodplain complexity and surface metrics: Influences of scale and geomorphology. Geomorphology 245, 102-116. https://doi.org/10.1016/j.geomorph.2015.05.024

Sear, D. and Newson, M. (2004) The hydraulic impact and performance of a lowland rehabilitation scheme based on pool–riffle installation: the River Waveney, Scole, Suffolk, UK. River Research and Applications 20(7), 847-863. https://doi.org/10.1002/rra.791

Shaheed, R. (2016) 3D Numerical Modelling of Secondary Current in Shallow River Bends and Confluences, Université d'Ottawa/University of Ottawa, Ottawa, Canada. http://dx.doi.org/10.20381/ruor-6164

Stewardson, M. (2005) Hydraulic geometry of stream reaches. Journal of Hydrology 306(1-4), 97-111. https://doi.org/10.1016/j.jhydrol.2004.09.004

Stewardson, M., Datry, T., Lamouroux, N., Pella, H., Thommeret, N., Valette, L. and Grant, S. (2016) Variation in reach-scale hydraulic conductivity of streambeds. Geomorphology 259, 70-80. https://doi.org/10.1016/j.geomorph.2016.02.001

Stonedahl, S.H. (2011) Investigation of the Effect Multiple Scales of Topography on Hyporheic Exchange, Northwestern University, Illinois, United States.

841 Stonedahl, S.H., Harvey, J.W. and Packman, A.I. (2013) Interactions between hyporheic flow produced by
842 stream meanders, bars, and dunes. Water Resources Research 49(9), 5450-5461.
843 https://doi.org/10.1002/wrcr.20400

844 Strom, M.A., Pasternack, G.B. and Wyrick, J.R. (2016) Reenvisioning velocity reversal as a diversity of
845 hydraulic patch behaviours. Hydrological Processes 30(13), 2348-2365. https://doi.org/10.1002/hyp.10797

846 Thibodeaux, L.J. and Boyle, J.D. (1987) Bedform-generated convective transport in bottom sediment.
847 Nature 325(6102), 341. https://doi.org/10.1038/325341a0

848 Tonina, D. and Buffington, J.M. (2007) Hyporheic exchange in gravel bed rivers with pool-riffle
849 morphology: Laboratory experiments and three-dimensional modeling. Water Resources Research 43(1).
850 https://doi.org/10.1029/2005WR004328

851 Tonina, D. and Buffington, J.M. (2009) Hyporheic exchange in mountain rivers I: Mechanics and
852 environmental effects. Geography Compass 3(3), 1063-1086. https://doi.org/10.1111/j.1749-
853 8198.2009.00226.x

854 Tonina, D. and Buffington, J.M. (2011) Effects of stream discharge, alluvial depth and bar amplitude on
855 hyporheic flow in pool-riffle channels. Water Resources Research 47(8).
856 https://doi.org/10.1029/2010WR009140

857 Trainor, K. and Church, M. (2003) Quantifying variability in stream channel morphology. Water Resources
858 Research 39(9). https://doi.org/10.1029/2003WR001971

859 Trauth, N., Schmidt, C., Maier, U., Vieweg, M. and Fleckenstein, J.H. (2013) Coupled 3-D stream flow
860 and hyporheic flow model under varying stream and ambient groundwater flow conditions in a pool-riffle
861 system. Water Resources Research 49(9), 5834-5850. https://doi.org/10.1002/wrcr.20442

862 Trauth, N., Schmidt, C., Vieweg, M., Maier, U. and Fleckenstein, J.H. (2014) Hyporheic transport and
863 biogeochemical reactions in pool-riffle systems under varying ambient groundwater flow conditions.
864 Journal of Geophysical Research: Biogeosciences 119(5), 910-928. https://doi.org/10.1002/2013JG002586

865 Trauth, N., Schmidt, C., Vieweg, M., Oswald, S.E. and Fleckenstein, J.H. (2015) Hydraulic controls of in-
866 stream gravel bar hyporheic exchange and reactions. Water Resources Research 51(4), 2243-2263.
867 https://doi.org/10.1002/2014WR015857

868 Tuttle, A.K., McMillan, S.K., Gardner, A. and Jennings, G.D. (2014) Channel complexity and nitrate
869 concentrations drive denitrification rates in urban restored and unrestored streams. Ecological engineering
870 73, 770-777. https://doi.org/10.1016/j.ecoleng.2014.09.066

871 Wade, R.J., Rhoads, B.L., Rodríguez, J., Daniels, M., Wilson, D., Herricks, E.E., Bombardelli, F., Garcia,
872 M. and Schwartz, J. (2002) INTEGRATING SCIENCE AND TECHNOLOGY TO SUPPORT STREAM
873 NATURALIZATION NEAR CHICAGO, ILLINOIS 1. JAWRA Journal of the American Water Resources
874 Association 38(4), 931-944.

875 Ward, A.S. (2016) The evolution and state of interdisciplinary hyporheic research. Wiley Interdisciplinary
876 Reviews: Water 3(1), 83-103. https://doi.org/10.1002/wat2.1120

877 Wheaton, J.M., Brasington, J., Darby, S.E., Merz, J., Pasternack, G.B., Sear, D. and Vericat, D. (2010)
878 Linking geomorphic changes to salmonid habitat at a scale relevant to fish. River Research and Applications
879 26(4), 469-486. https://doi.org/10.1002/rra.1305

880 White, J.Q., Pasternack, G.B. and Moir, H.J. (2010) Valley width variation influences riffle–pool location
881 and persistence on a rapidly incising gravel-bed river. Geomorphology 121(3-4), 206-221.
882 https://doi.org/10.1016/j.geomorph.2010.04.012

883 Whiteway, S.L., Biron, P.M., Zimmermann, A., Venter, O. and Grant, J.W. (2010) Do in-stream restoration
884 structures enhance salmonid abundance? A meta-analysis. Canadian Journal of Fisheries and Aquatic
885 Sciences 67(5), 831-841. https://doi.org/10.1139/F10-021

886 Wohl, E. (2016) Spatial heterogeneity as a component of river geomorphic complexity. Progress in Physical
887 Geography 40(4), 598-615. https://doi.org/10.1177/0309133316658615

888 Wu, F.C. and Yeh, T.H. (2005) Forced bars induced by variations of channel width: Implications for
889 incipient bifurcation. Journal of Geophysical Research: Earth Surface 110(F2).
890 https://doi.org/10.1029/2004JF000160

891 Wyrick, J.R. and Pasternack, G.B. (2016) Revealing the natural complexity of topographic change
892 processes through repeat surveys and decision-tree classification. Earth Surface Processes and Landforms
893 41(6), 723-737. https://doi.org/10.1002/esp.3854

894 Xu, J. (2004) Comparison of hydraulic geometry between sand-and gravel-bed rivers in relation to channel
895 pattern discrimination. Earth Surface Processes and Landforms: The Journal of the British
896 Geomorphological Research Group 29(5), 645-657. https://doi.org/10.1002/esp.1059

897 Yang, C.T. (1971) Formation of riffles and pools. Water Resources Research 7(6), 1567-1574.
898 https://doi.org/10.1029/WR007i006p01567

899 Zheng, L., Cardenas, M.B., Wang, L. and Mohrig, D. (2019) Ripple Effects: Bed Form Morphodynamics
900 Cascading Into Hyporheic Zone Biogeochemistry. Water Resources Research 55(8), 7320-7342.
901 https://doi.org/10.1029/2018WR023517

902 Zhou, T. and Endreny, T.A. (2013) Reshaping of the hyporheic zone beneath river restoration structures:
903 Flume and hydrodynamic experiments. Water Resources Research 49(8), 5009-5020.
904 https://doi.org/10.1002/wrcr.20384

905

906